Transportin acts to regulate mitotic assembly events by target binding rather than Ran sequestration

Cyril Bernis[a], Beth Swift-Taylor[a], Matthew Nord[a], Sarah Carmona[a], Yuh Min Chook[b], and Douglass J. Forbes[a]

[a]Section of Cell and Developmental Biology, Division of Biological Sciences 0347, University of California–San Diego, La Jolla, CA 92093-0347; [b]Department of Pharmacology, University of Texas Southwestern Medical Center, Dallas, TX 75390-9041

ABSTRACT The nuclear import receptors importin β and transportin play a different role in mitosis: both act phenotypically as spatial regulators to ensure that mitotic spindle, nuclear membrane, and nuclear pore assembly occur exclusively around chromatin. Importin β is known to act by repressing assembly factors in regions distant from chromatin, whereas RanGTP produced on chromatin frees factors from importin β for localized assembly. The mechanism of transportin regulation was unknown. Diametrically opposed models for transportin action are as follows: 1) indirect action by RanGTP sequestration, thus down-regulating release of assembly factors from importin β, and 2) direct action by transportin binding and inhibiting assembly factors. Experiments in *Xenopus* assembly extracts with M9M, a super-affinity nuclear localization sequence that displaces cargoes bound by transportin, or TLB, a mutant transportin that can bind cargo and RanGTP simultaneously, support direct inhibition. Consistently, simple addition of M9M to mitotic cytosol induces microtubule aster assembly. ELYS and the nucleoporin 107–160 complex, components of mitotic kinetochores and nuclear pores, are blocked from binding to kinetochores in vitro by transportin, a block reversible by M9M. In vivo, 30% of M9M-transfected cells have spindle/cytokinesis defects. We conclude that the cell contains importin β and transportin "global positioning system"or "GPS" pathways that are mechanistically parallel.

INTRODUCTION

Mitosis is a precisely controlled process that requires multiple mechanisms for that control. Mitotic kinases and phosphatases act to regulate the sequential changes between different mitotic events. For example, nuclear disassembly and chromatin condensation are set in motion at prophase by the mitotic kinase Cdk1/cyclin B. In contrast, mitosis-specific ubiquitination and proteolysis drive the transition from metaphase to anaphase. The foregoing enzymes all regulate the *timing* of mitotic events. However, the *spatial* regulation of assembly of mitotic structures involves unexpected players: the karyopherins and RanGTP. Importin β and importin α, together with the small GTPase Ran, act as dueling regulators to determine where mitotic spindle assembly occurs, causing this system to be referred to as a cellular "GPS" or "global positioning system" (Kalab *et al.*, 1999; Kalab and Heald, 2008; Gruss *et al.*, 2001; Nachury *et al.*, 2001; Wiese *et al.*, 2001; Askjaer *et al.*, 2002; Arnaoutov and Dasso, 2003; Di Fiore *et al.*, 2004; Ems-McClung *et al.*, 2004; Ciciarello *et al.*, 2007; Clarke and Zhang, 2008; Yokoyama *et al.*, 2008; Bird *et al.*, 2013). Late in mitosis, the same system also controls where nuclear membrane and nuclear pore assembly occur in the cell (Marshall and Wilson, 1997; Wiese *et al.*, 1997; Wilde *et al.*, 2001; Askjaer *et al.*, 2002; Hetzer *et al.*, 2002; Zhang *et al.*, 2002a,b; Harel *et al.*, 2003a; Harel and Forbes, 2004; Ryan *et al.*, 2003, 2007;

Walther et al., 2003b; Clarke and Zhang, 2004; Hachet et al., 2004; Prunuske and Ullman, 2006; Rotem et al., 2009). Importin β was believed to be the only karyopherin that plays this mitotic role, but subsequent work on the karyopherin transportin (Lau et al., 2009) demonstrated that it too spatially regulates the same mitotic assembly events.

Integral to the above studies was the use of mitotic and interphase cytosolic extracts derived from *Xenopus laevis* eggs. These provided cell cycle phase–specific extracts in which one could reconstitute either the assembly of spindles in mitotic extracts or the assembly of nuclei with functional nuclear membranes and pores in interphase extracts, all in the space of an hour (Forbes et al., 1983; Finlay and Forbes, 1990; Lohka and Masui, 1983, 1985; Newport, 1987; Newport and Spann, 1987; Wilson and Newport, 1988; Pfaller et al., 1991; reviewed in Newmeyer and Wilson, 1991; Chan and Forbes, 2006; Maresca and Heald, 2006; Cross and Powers, 2008, 2009). Thus the extracts serve as excellent assays in which to test how karyopherin regulation of assembly occurs mechanistically.

To understand how karyopherins act in mitosis, knowledge of their action in interphase serves as an invaluable guide. Nuclear transport is governed by the small GTPase Ran and a family of nuclear transport receptors or karyopherins 90–130 kDa in size (Melchior et al., 1993; Melchior and Gerace, 1998; Izaurralde et al., 1997; Ben-Efraim et al., 2009; Wente and Rout, 2010). Individual karyopherins, of which there are 22 in humans, are generally tasked either for nuclear import or nuclear export and often have specific cargoes (Aitchison et al., 1996; Lee and Aitchison, 1999; Chook and Blobel, 2001; Marelli et al., 2001a,b; Fried and Kutay, 2003; Chook and Suel, 2011). All karyopherins are composed primarily of HEAT repeats (huntingtin-elongation factor 3-A subunit of protein phosphatase 2A-TOR1 lipid kinase repeats), but in fact have low sequence homology to one another except for a common N-terminal RanGTP-binding domain.

The active form of Ran, RanGTP, is uniquely localized within the nucleus, and this sets up the directionality of transport (Izaurralde et al., 1997; Kalab et al., 2002, 2006). This is due to the fact that RCC1, the Ran guanine-exchange factor (Ran-GEF), is a chromatin-bound protein (Ohtsubo et al., 1989; Bischoff and Ponstingl, 1991a,b; Ren et al., 1993; Gorlich et al., 1996; Gorlich and Kutay, 1999; Melchior and Gerace, 1998; Moore et al., 2002; Li et al., 2003; Clarke and Zhang, 2004). The inactive form, RanGDP, is the primary form found in the cytoplasm, as a result of the localization of RanGAP to the cytoplasmic face of the nuclear pore and the cytoplasm (Bischoff et al., 1994; Gorlich et al., 1996; Bischoff and Gorlich, 1997; Kehlenbach et al., 1999, 2001). This asymmetry of RanGAP and RanGEF creates a sharp gradient of active and inactive Ran across the nuclear envelope (Kalab et al., 2002, 2006; Di Fiore et al., 2004).

Import karyopherins recognize cargoes in the cytoplasm via receptor-specific nuclear localization sequences (NLSs). The receptors then transport their cargoes into the nucleus by moving through the nuclear pore via interaction with a set of phenylalanine-glycine (FG) repeat–containing nuclear pore proteins (FG nucleoporins [Nups]; Powers et al., 1997; Bayliss et al., 2000b,c; Ben-Efraim and Gerace, 2001; Ben-Efraim et al., 2009; Chook and Blobel, 2001; Chook and Suel, 2011; Blevins et al., 2003; Strawn et al., 2004; Conti et al., 2006; Frey et al., 2006; Walde and Kehlenbach, 2010; Xu et al., 2010). Once inside the nucleus, import receptors bind to RanGTP, which causes the release of cargo and completion of import.

Importin β (karyopherin-β1) and transportin (karyopherin-β2) are by far the best studied of the import karyopherins. Each recognizes distinct cargoes in the cytoplasm, although some cargoes

are recognized by both (Gorlich et al., 1994, 1995; Gorlich and Kutay, 1999; Conti et al., 1998; Harel and Forbes, 2004; Chook and Suel, 2011; Kimura et al., 2013). Importin β, a 96-kDa protein, imports a wide range of proteins with positively charged "classical" NLSs. Often it uses the adaptor protein importin α to recognize these classical NLSs (Gorlich et al., 1995; Goldfarb et al., 2004; Mosammaparast and Pemberton, 2004).

Transportin, the subject of this study, functions without an adaptor. Transportin serves as the import receptor for a large class of mRNA-binding proteins, as well as for other proteins, including the medically relevant Fused in Sarcoma protein (Chook and Suel, 2011; Zhang and Chook, 2012; Dormann et al., 2012). Transportin has additionally been shown to be the import receptor for exogenous DNA entry into the nucleus, an entry relevant to gene therapy (Lachish-Zalait et al., 2009). Interestingly, two human papilloma viruses have evolved to inhibit transportin-mediated import of cellular cargoes; presumably this frees up nuclear materials for viral replication (Nelson et al., 2002).

The NLSs recognized by transportin vary in sequence and length but often contain a proline–tyrosine (PY) dipeptide motif. Two subclasses of PY-NLSs, hydrophobic (h) and basic (b), have been defined. The hPY-NLS contains a hydrophobic motif preceding an $R/H/K/X_{(2-5)}PY$ motif, whereas the bPY-NLS contains basic amino acid residues preceding the $R/H/K/X_{(2-5)}PY$ motif (Lee et al., 2006; Cansizoglu and Chook, 2007). Other transportin-binding cargoes contain dipeptide motifs homologous to the PY, such as PG, PL, or PV (Lee and Aitchison, 1999; Rebane et al., 2004; Suel et al., 2008; Chook and Suel, 2011; Lau et al., 2009). PY-like NLSs are not found in all transportin cargoes, however, as some cargoes contain instead a recently characterized BIB motif (a Lys/Arg-rich segment), which can bind either to transportin or importin β (Kimura et al., 2013).

Crystal structure analysis of transportin revealed that transportin undergoes structural changes during the import cycle. Transportin consists of two perpendicular arches of 20 HEAT repeats total (H1–H20; Figure 1B; Andrade and Bork, 1995; Chook and Blobel, 1999; Cansizoglu and Chook, 2007; Groves et al., 1999; Conti et al., 2006). The N-terminal arch of transportin contains the RanGTP-binding site, and the C-terminal arch contains the NLS/cargo-binding site. A long 62–amino acid acidic loop termed the H8 loop is inserted in HEAT repeat 8 and connects the two halves. The H8 loop normally protrudes and is disordered in either empty or NLS-bound transportin (Chook et al., 2002; Cansizoglu and Chook, 2007; Lee et al., 2006). When RanGTP binds to transportin, however, the H8 loop undergoes a conformational change, moving into the cargo-binding site and causing the release of the cargo (Figure 1B; Chook and Blobel, 2001; Chook et al., 2002; Cansizoglu and Chook, 2007; Lee et al., 2006).

A novel and potent molecular tool that can counteract this process was created by combining parts of the two types of PY-NLSs to form a chimeric peptide termed M9M (Figure 1A; Cansizoglu et al., 2007). M9M was generated by fusion of the N-terminal hydrophobic segment of the heterogeneous nuclear ribonucleoprotein (hnRNP) A1 NLS and the C-terminal $R/H/K/X_{(2-5)}PY$ motif from the basic-PY NLS of hnRNP M (Figure 1A). Representing the binding "hotspots" of their respective PY-NLSs, the avidity effect of combination of the two hotspots resulted in the chimeric M9M peptide, which has a significantly increased affinity for transportin that is ~200-fold tighter than its affinity for natural PY-NLSs or RanGTP (Chook et al., 2002; Cansizoglu et al., 2007). As a result, M9M acts as a Ran-resistant inhibitor of transportin. M9M prevents transportin from binding its endogenous cargoes by replacing native cargoes already bound to transportin (Cansizoglu et al.,
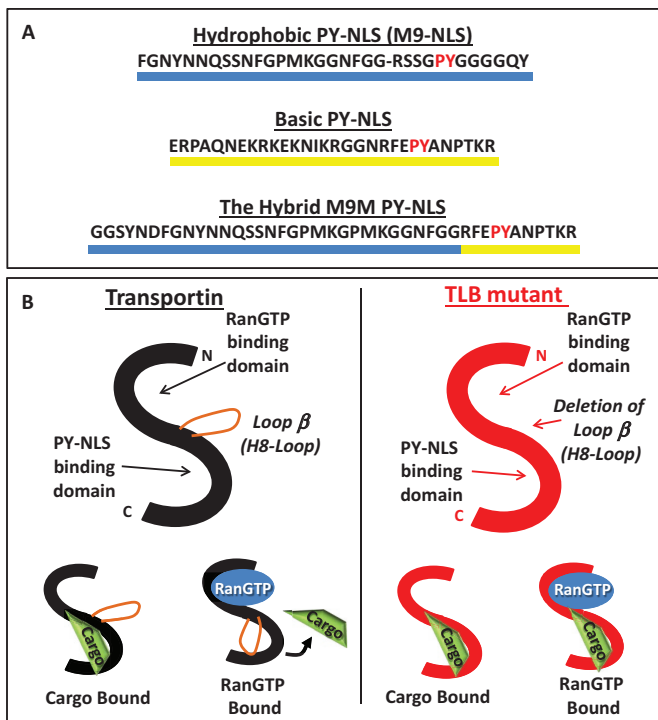
FIGURE 1: Molecular tools for probing the mechanism of action of transportin in mitosis. (A) M9M is a synthetic hybrid PY-NLS peptide capable of binding to transportin with 200-fold binding strength relative to the M9 NLS (Cansizoglu *et al.*, 2007). M9 is the NLS found in hnRNP A1 (Siomi and Dreyfuss, 1995; Nakielny *et al.*, 1996; Pollard *et al.*, 1996; Iijima *et al.*, 2006; Lee *et al.*, 2006); it is in the class of hydrophobic PY-NLSs. Also shown is the basic PY-NLS found in hnRNP M. M9M is a hybrid constructed from these hydrophobic and basic PY-NLSs. In all experiments, M9M is used in a recombinant form of MBP-M9M, where M9M is fused to MBP for ease of purification and use. (B) Wild-type transportin recognizes and binds cargo containing a PY-NLS; when the transportin:cargo complex encounters and binds RanGTP, the H8 loop moves to displace the cargo. The transportin TLB mutant lacks the H8 loop, and, as such, when RanGTP interacts with the cargo-laden complex, the cargo is not displaced. This allows TLB to be bound to cargo and RanGTP simultaneously. This schematic representation is an adaptation of the description provided in Chook *et al.* (2002).

2007; Dormann *et al.*, 2012). Small-molecule inhibitors of karyopherins have previously proven valuable for inhibiting karyopherins, including leptomycin B, which inhibits cargo binding to exportin1/Crm1, and karyostatin 1A and importazole, which inhibit RanGTP binding to importin β (Fornerod *et al.*, 1997; Ambrus *et al.*, 2010; Hintersteiner *et al.*, 2010; Soderholm *et al.*, 2011; Bird *et al.*, 2013). In this study, we use the M9M peptide to probe the role of transportin in mitosis.

During mitosis, importin β and transportin play an interesting and entirely different role from that of nuclear import. In mitosis, formation of a spindle and, later, a nuclear envelope is clearly desirable but only around chromosomes. Importin β has been coopted by evolution to act as a critical negative regulator for these mitotic assembly events. How does this work mechanically? Owing to the presence of the RanGEF RCC1 on chromatin, a RanGTP "cloud" exists only around chromatin (Kalab and Heald, 2008). It has been found that importin β acts to bind and mask required spindle assembly factors (SAFs) everywhere except in the vicinity of chromatin. There RanGTP is produced and disrupts any

nearby importin β:SAF complexes, freeing the SAFs for spindle assembly but only around the mitotic chromosomes (Nachury *et al.*, 2001; Wiese *et al.*, 2001; Askjaer *et al.*, 2002; Harel and Forbes, 2004; Kalab and Heald, 2008). Among the SAFs regulated by importin β are the nuclear mitotic apparatus protein NuMA (Nachury *et al.*, 2001), the microtubule-binding protein TPX2 (Gruss *et al.*, 2001), and lamin B, which serves as part of the matrix that organizes the spindle (Tsai *et al.*, 2006; Kalab and Heald, 2008). Proceeding into telophase, nuclear membrane assembly and nuclear pore assembly also employ importin β and RanGTP as dueling regulators (Askjaer *et al.*, 2002; Zhang *et al.*, 2002b; Clarke and Zhang, 2004; Harel *et al.*, 2003a; Walther *et al.*, 2003b; Ryan *et al.*, 2007; Delmar *et al.*, 2008; Kutay and Hetzer, 2008; Rasala *et al.*, 2008; Rotem *et al.*, 2009; Wandke and Kutay, 2013; reviewed in Dasso, 2001; Quimby and Dasso, 2003; Di Fiore *et al.*, 2004; Harel and Forbes, 2004; Mosammaparast and Pemberton, 2004; Ciciarello *et al.*, 2007; Kalab and Heald, 2008). Together importin β and RanGTP act to ensure that nuclear membranes and pores form only around chromatin, doing so in the correct place and in the correct amount.

We found in a previous study that the distantly related karyopherin transportin also functions as a negative regulator of spindle, nuclear membrane, and nuclear pore assembly (Lau *et al.*, 2009). The mode of transportin's action has been unknown. Two diametrically opposed hypothetical models could explain transportin's mechanism of action. In the first, transportin could act to down-regulate importin β by physically sequestering RanGTP. In this mode, transportin, by binding and decreasing the concentration of available RanGTP, would thereby reduce importin β's ability to release assembly factors around chromatin. In an alternate mechanism, transportin could act directly by inhibiting one or more structure-specific assembly factors everywhere except in the vicinity of chromatin where RanGTP is produced. The focus of the present study is to use potent mutant forms of the transportin NLS and of transportin itself to distinguish between these different regulatory mechanisms for spindle assembly, nuclear membrane assembly, and nuclear pore assembly.

RESULTS

Transportin and importin β are present in equivalent concentrations

Mitotic and interphase cytosolic extracts derived from *X. laevis* eggs provided a convenient way to test the Ran competition and direct inhibition models (Newmeyer and Wilson, 1991; Chan and Forbes, 2006; Maresca and Heald, 2006; Cross and Powers, 2008, 2009). In addition, the effects of recombinant proteins and potential inhibitors can easily be tested. Importin β exists in *Xenopus* egg extracts in micromolar concentration (Gorlich and Rapoport, 1993). The concentration of endogenous transportin was unknown. If transportin were, for example, 10-fold lower in concentration than importin β, a Ran competition mode by which transportin effectively modulates RanGTP would be less likely. Thus comparative quantitation was done by comparing concentrations of endogenous *Xenopus* importin β and transportin in egg extracts to a dilution series of recombinant importin β and transportin purified from *Escherichia coli* using immunoblot analysis. The concentration of endogenous importin β in interphase *Xenopus* egg extracts was found to average 6.5 μM (Supplemental Figure S1A), whereas that of endogenous transportin averaged 7 μM (Supplemental Figure S1B). We conclude that endogenous importin β and transportin are present in comparable concentrations in interphase *Xenopus* egg extracts.

The super NLS M9M shows high specificity for *Xenopus* transportin in interphase and mitotic extracts

M9M, the human chimeric PY-NLS peptide, has such high binding affinity ($K_d \approx 100$ pM) that it acts as a potent and specific inhibitor of human transportin function in vivo. To ask whether M9M shows a similar high binding affinity for *Xenopus* transportin, as well as a lack of affinity for importin β, we performed direct pull downs using recombinant NLS baits. As baits, maltose-binding protein (MBP), MBP fused to the hnRNPA1-derived NLS M9 (MBP-M9), or MBP fused to the transportin inhibitor M9M (MBP-M9M) were each bound to beads (Cansizoglu and Chook, 2007). Recombinant *Xenopus* glutathione S-transferase (GST)–transportin, *Xenopus* GST-importin β, or GST (100 μg) was incubated with each set of beads and then pulled down. On comparing the input samples of GST-transportin, GST-importin β, and GST (Supplemental Figure S1C, lanes 10–12) to the experimental bead pull downs (lanes 1–9), the only interaction we observed was GST-transportin and MBP-M9M (Supplemental Figure S1C, lane 3). No interaction of MBP-M9M was seen with importin β (Supplemental Figure S1C, lane 6). This demonstrated that M9M both specifically and directly binds to *Xenopus* transportin.

To test the interaction of M9M with endogenous *Xenopus* transportin in the context of interphase or mitotic *Xenopus* egg extracts, we again bound MBP, MBP-M9, or MBP-M9M (130 μg) as bait to beads. We then added 100 μl of interphase or mitotic egg extract to the beads. After removing any unbound proteins, we analyzed the binding of transportin or importin β by immunoblotting (Supplemental Figure S1D). The MBP control beads showed no affinity for endogenous *Xenopus* transportin or importin β in either interphase or mitotic extracts (Supplemental Figure S1D, lane 1). The original hnRNP A1–derived M9-NLS present in MBP-M9 *comparatively* pulled down only a very small amount of endogenous transportin from both extracts but did not pull down importin β (Supplemental Figure S1D, lane 2). In contrast, MBP-M9M strongly pulled down endogenous transportin from both interphase and mitotic extracts (Supplemental Figure S1D, lane 3). M9M beads did not pull down importin β. We conclude that M9M interacts strongly and specifically with both mitotic and interphase *Xenopus* transportin, mirroring its action in human cells. These experiments are the first to show affinity of M9M for transportin in mitosis.

Inhibition of transportin in HeLa cells induces defects in spindle assembly and cytokinesis

Transfection of M9M into interphase HeLa cells causes a functional block to nuclear import mediated by transportin (Cansizoglu et al., 2007). We wanted to ask whether M9M would cause defects in mitotic events. We transfected the M9M super-NLS into HeLa cells and monitored the effect on events in mitosis and cytokinesis. HeLa cells were transfected overnight with myc-tagged control MBP or MBP-M9M in pCS2+ myc-tagged vectors. Transfected cells were detected with a tetramethylrhodamine isothiocyanate (TRITC)–anti-myc antibody. Microtubule structures were visualized with fluorescein isothiocyanate (FITC)–anti-tubulin antibody, and DNA was visualized with 4′,6-diamidino-2-phenylindole (DAPI). Microtubule structures in untransfected cells were assessed as an additional control.

Strikingly, ~30% of the cells transfected with the transportin inhibitor M9M showed defects in either mitosis or cytokinesis. These results are summarized in Figure 2, A–E, and quantitated in Figure 2F. In both control conditions (MBP-transfected as well as untransfected cells), ~3% of the cells contained microtubule midbodies (Figure 2F, midbodies, gray bar). This indicated that normally 3% of the HeLa cells under our control conditions are in cytokinesis. A midbody is a normal microtubule-containing structure spanning the region at the

junction of cells as they are completing cytokinesis (arrow, Figure 2A, tubulin; Hu et al., 2012). Strikingly, ~18% of M9M-transfected cells contained midbodies (Figure 2, A and F, midbodies, red bar). Moreover, ~72% of these M9M-transfected, midbody-containing cells had DNA bridges underlying their microtubule midbody (13% of total transfected cells; Figure 2, B, DNA, and F, DNA bridges, red bar). None of the control cells contained DNA bridges (Figure 2F, DNA bridges, gray bar).

In addition to the above, another 6% of M9M-transfected cells were multinucleate, whereas <1% of control cells (MBP-transfected or untransfected) showed a multinucleate phenotype (Figure 2, C and F, multinucleate cells, red bar). The observation of a multinucleate cell indicates that a cell attempted to divide and failed, and the two daughter cells were never able to separate. Together these aberrant structures—that is, increased midbodies, the presence of DNA bridges, and increased multinucleate cells—indicate that cells transfected with M9M have problems completing cytokinesis.

Another striking defect observed in M9M-transfected cells was an alteration not in the number, but in the morphology of their mitotic spindles. Normally, ~6% of control cells show a mitotic spindle (MBP-transfected or nontransfected cells). Fewer than 1 in 100 of these control cells with spindles have any significant problem with their spindle morphology (Figure 2, F, CTL, red and gray bars, and G). However, in M9M-transfected cells, although again 6% had a mitotic spindle, ~80% of these were defective spindles (Figure 2, F, abnormal spindles, +M9M, red bar, and G). Instead of a normal bipolar spindle, these cells had chaotic, disorganized microtubule structures around the DNA (Figure 2E, green; compare to normal spindle, Figure 2D, green).

In summary, cells that were transfected with M9M showed clear defects in both mitosis and cytokinesis. These defects indicate that, when M9M inhibits transportin, cells are unable to carry out mitosis normally. The defects could be due to loss of transportin's ability to regulate spindle assembly during *mitosis*. However, with this in vivo experiment we could not exclude that the mitotic defects result from an inhibition of transportin-mediated *import* of essential spindle assembly factors or chromosomal proteins required later for correct mitosis or even from the activation of the abscission checkpoint (i.e., where a defect in nuclear pore assembly activates the Aurora-B abscission checkpoint, leading to increased midbodies; Mackay et al., 2010; Mackay and Ullman, 2011). Therefore, to examine the mitotic effects of transportin inhibition independent of any interphase or import role, we needed to use *Xenopus* cell cycle–specific mitotic extracts, as described next.

Addition of M9M to an in vitro spindle assembly assay: M9M mimics RanGTP in inducing larger spindles, multipolar spindles, and chromatin-free asters

Previous studies in our lab showed that transportin can function as a negative regulator of spindle assembly. That is, addition of excess transportin to mitotic *Xenopus* egg extracts inhibits spindle assembly (Lau et al., 2009). Above, we found that inhibition of transportin by M9M in HeLa cells also caused striking defects in mitosis and cytokinesis. To begin to address the question of whether transportin functions in spindle assembly *indirectly* (by sequestering Ran) or *directly* (by binding and masking spindle assembly factors), we used interphase and mitotic extracts derived from *Xenopus* eggs.

For this analysis, *Xenopus* sperm chromatin was incubated in an interphase extract for 2 h to allow nuclei to form and the chromatin to be replicated. After this, 10 μl of the interphase reaction containing nuclei was mixed with 15 μl of freshly prepared mitotic extract to induce mitosis. The reaction was also supplemented
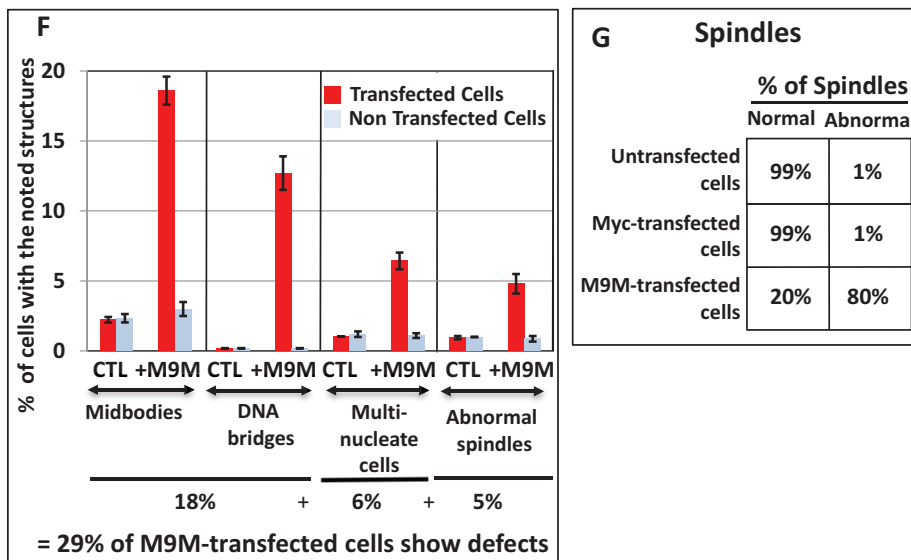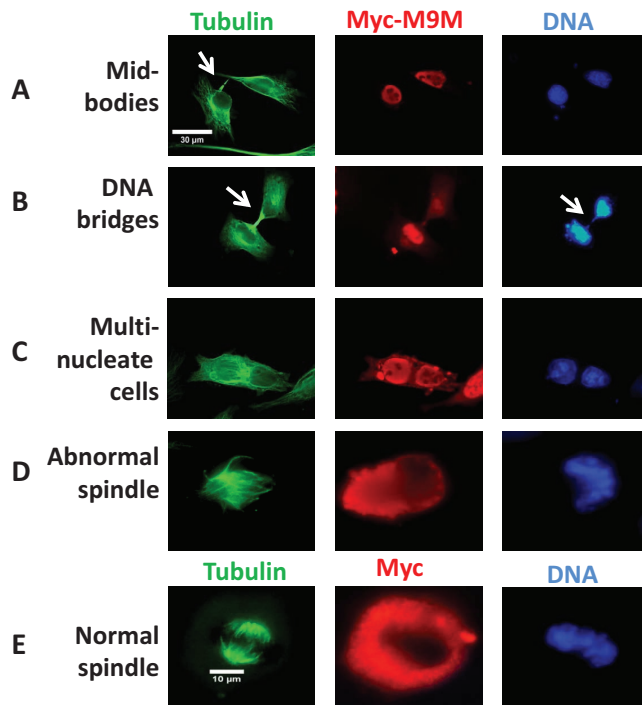
FIGURE 2: M9M inhibition of transportin in HeLa cells causes defects in mitosis. HeLa cells were transfected for 24 h with mammalian expression vectors containing the myc-tagged MBP constructs MBP, MBP-M9, and MBP-M9M. The transfection of the M9M construct caused clear defects in cytokinesis. Abnormal structures observed included (A) excess midbodies, (B) DNA bridges between cells accompanying said midbodies, and (C) multinucleate cells. Few of these defects were observed in cells that were untransfected or transfected with myc-tagged MBP (see F). In addition, in cells showing mitotic spindles, a large fraction had defective spindles after MBP-M9M plasmid transfection (D), whereas those transfected with MBP constructs showed normal spindles (E). Tubulin was detected with a FITC-labeled anti-tubulin antibody (green), myc-construct transfected cells were visualized with a TRITC-labeled anti-myc antibody (red), and DNA was visualized with DAPI (blue). (F) Quantification of the different aberrant structures observed in HeLa cells transfected with MBP constructs was performed and graphed. In cells transfected with MBP-M9M, 18% showed midbodies (+M9M, red bar), as compared with <3% of nontransfected cells on the same coverslip (+M9M, gray bar) or cells transfected with MBP (CTL, red bar, transfected; gray bar, untransfected on same coverslip). Thirteen percent of the MBP-M9M–transfected cells showing midbodies also showed DNA bridges (DNA bridges, +M9M, red bar), as opposed to no detectable DNA bridges in the MBP-transfected control or the nontransfected cells. Another 6% of the MBP-M9M–transfected cells were multinucleate (multinucleate cells, +M9M, red bar), as opposed to <1% of the MBP-transfected control or

with rhodamine-labeled tubulin at this time, and this was designated $t = 0$ min for the mitotic reaction. After 5 min, an aliquot of the reaction was checked to verify that mitotic breakdown of the nuclear envelopes, chromosome condensation, and initiation of aster formation adjacent to the chromatin had occurred (Figure 3, 5-min time point). At this time, the reactions were supplemented with control protein, MBP-M9M, or RanQ69L-GTP and incubated for 1 h. An aliquot (2 μl) of each spindle assembly reaction was fixed on glass slides and examined by fluorescence microscopy. Microtubules were visualized via rhodamine-labeled tubulin, and chromatin was visualized by Hoechst DNA dye.

Following addition of control protein, the dominant structures observed in the reaction were normal bipolar spindles (77%; Figure 3A, +MBP/Ctl, top). Also observed but in lesser amounts in the control reaction were weak spindles (13%), half-spindles (5%), and condensed chromatin lacking any associated microtubules (4%). This range of structures is commonly observed in in vitro spindle assembly assays (see, for example, Orjalo *et al.*, 2006; Lau *et al.*, 2009).

When MBP-M9M (10 μM) was added to a spindle assembly assay, 45% normal bipolar spindles were observed (Figure 3B, +M9M, top). However, three unusual structures that formed in the M9M reaction differed greatly from those formed in the control. Very large spindles, assembled around a larger than normal amount of chromatin, were observed as 15% of the structures (Figure 3B, +M9M, second from top). Clusters of asters, which are groups of spontaneous microtubule structures nucleated without associated chromatin, represented 26% of the total (Figure 3B, +M9M, second from bottom). In addition, 8% of the M9M-induced structures were multipolar spindles (Figure 3B, +M9M, bottom), whereas 6% were chromatin not associated with microtubules (unpublished data).

Surprisingly, these M9M results mirrored those that occur upon addition of excess RanQ69L-GTP to mitotic *Xenopus* extracts. RanQ69L is a constitutively active mutant form of Ran, able to bind but not

nontransfected cells. In all of our transfections, 6% of the total cells had mitotic spindles. (G) However, whereas only ~1% of the spindles in control myc-MBP– transfected cells and 1% of the spindles in nontransfected cells were abnormal, we found that 80% of the spindles in MBP-M9M– transfected cells were abnormal (see also abnormal spindles in F).
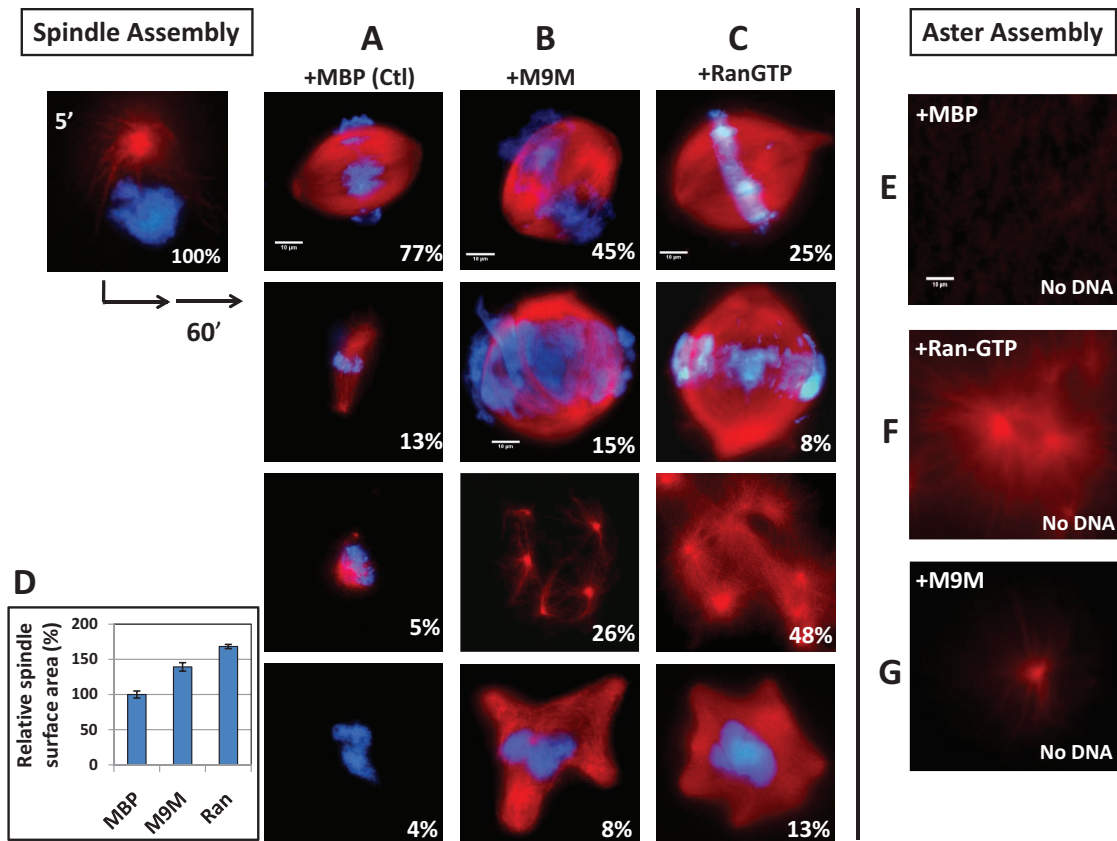
FIGURE 3: M9M addition to mitotic extracts mirrors Ran GTP in causing large spindles, free asters, and multipolar spindles. (A–C) Freshly prepared interphase *Xenopus* egg extract was mixed with sperm chromatin; nuclei were allowed to form and the DNA to replicate for 2 h. Mitotic *Xenopus* extract was then added to convert it to a mitotic state. Rhodamine-labeled tubulin was added with recombinant MBP, MBP-M9M, or RanGTP (Ran Q69L-GTP) 5 min later. The resulting microtubule structures (red) were examined at 60 min using fluorescence microscopy; chromatin was visualized with Hoechst DNA dye (blue). (A) Control condition: after MBP addition (10 μM), the majority of condensed chromatin structures (77%) showed strong bipolar spindles. Rarer structures included weak bipolar spindles (13%), half-spindles (5%), and chromatin with no associated microtubules (4%). (B) When MBP-M9M (10 μM) was added, 45% of the structures observed were normally shaped bipolar spindles of slightly increased size. However, now we also observed very large bipolar spindles with a larger than normal complement of DNA (15%), clusters of asters with no associated chromatin (26%), multipolar spindles (8%), and chromatin with no associated microtubules (6%; not shown). (C) When RanQ69L-GTP (10 μM) was instead added, we observed normally shaped bipolar spindles of slightly larger size (25%), very large spindles with much more associated DNA (8%), clusters of large asters with no associated chromatin (48%), and multipolar spindles (13%). Finally, 6% were chromatin with no associated microtubules (not shown). We note that the aforementioned M9M-induced asters are smaller than those induced in the RanGTP condition. (D) M9M, like RanGTP, promoted larger spindles in vitro. For A–C, representative images of the observed structures are shown. The percentage indicated on an image indicates the average percentage of that structure under that specific condition summarized from five replicate experiments; ~150 structures were counted for each condition for each experiment. The surface area of the normally shaped bipolar spindles from the MBP, M9M, and RanGTP conditions in A–C (top) were measured using ImageJ software (~40 spindles were measured per condition in three independent experiments). Overall, the bipolar spindles were ~40% larger with MBP-M9M addition and ~70% larger with RanQ69L-GTP addition than with MBP addition. (E–G) In the absence of chromatin, M9M, like RanGTP, induced aster assembly in vitro. *Xenopus* mitotic extract plus Energy Mix, but without added chromatin, was incubated with rhodamine-labeled tubulin and 10 μM MBP (control), 10 μM RanQ69L-GTP, or 10 μM MBP-M9M. No microtubule-containing structures were observed in the control (E; +MBP). RanGTP addition induced formation of microtubule asters (F; +Ran). RanGTP releases spindle assembly factors such as NuMa and TPX2 from importin (Zhang and Chook, 2012), causing impromptu microtubule nucleation (Gruss *et al.*, 2001; Nachury *et al.*, 2001). Microtubule asters also are seen here to form when MBP-M9M is added in the absence of chromatin (G; +M9M).

hydrolyze GTP. Addition of RanQ69L-GTP to mitotic extracts is known to cause widespread aster assembly, as well as larger bipolar spindles and multipolar spindles (Carazo-Salas *et al.*, 1999; Kalab *et al.*, 1999; Ohba *et al.*, 1999; Wilde and Zheng, 1999; Zhang *et al.*, 1999; Clarke and Zhang, 2008; Lau *et al.*, 2009; Gruss *et al.*, 2001; Nachury *et al.*, 2001; Ribbeck *et al.*, 2006; Cross and Powers, 2011). When excess RanQ69L-GTP was added (10 μM,

Figure 3C), we observed ~25% bipolar spindles, ~8% very large bipolar spindles associated with excess chromatin, and ~47% large clusters of asters. In addition, ~13% of the structures were multipolar spindles (Figure 3C, +RanGTP) and ~6% were chromatin not associated with microtubules (unpublished data). These RanGTP results are consistent with previous RanGTP findings cited earlier.

An additional notable effect of either M9M or RanQ69L-GTP addition was that the bipolar mitotic spindles that had a normal amount of DNA appeared to have a larger surface area (Figure 3, B and C, +M9M or +RanGTP, top). We quantified the surface area of ~40 spindles formed in the control condition (Figure 3A, +MBP, top) or without addition (unpublished data) and defined this as the baseline of 100% for surface area quantitation in Figure 3D. The normal bipolar spindles in the MBP-M9M condition, when similarly quantitated, were found to be 40% larger, whereas those formed in excess RanQ69L-GTP were 70% larger (Figure 3D).

We next added RanGTP or M9M to a *Xenopus* mitotic extract lacking chromatin. As stated earlier, Ran-Q69L-GTP causes spontaneous nucleation of microtubule asters in the absence of chromatin. A mitotic extract was incubated for 1 h with rhodamine-labeled tubulin and 10 µM MBP, RanQ69L-GTP, or MBP-M9M. In the control MBP condition, no microtubule structures were ever induced (Figure 3E, +MBP). With added Ran Q69L-GTP, aster formation was induced, as expected (Figure 3F, +Ran; Carazo-Salas *et al.*, 1999; Kalab *et al.*, 1999; Ohba *et al.*, 1999; Wilde and Zheng, 1999; Zhang *et al.*, 1999; Clarke and Zhang, 2008; Gruss *et al.*, 2001; Nachury *et al.*, 2001; Ribbeck *et al.*, 2006; Lau *et al.*, 2009; Cross and Powers, 2011). Strikingly, added MBP-M9M similarly caused aster formation (Figure 3G, +M9M), although fewer and of smaller size. Because M9M is known to displace cargo bound specifically to transportin (Cansizoglu *et al.*, 2007), it can be concluded that transportin was actively masking SAFs that were then freed by M9M and subsequently initiated microtubule aster formation. The striking M9M result strongly favors the direct inhibition model of transportin action.

We conclude that M9M, like RanGTP, acts as if it were a positive regulator of spindle assembly, inducing larger spindles, multipolar spindles, and even microtubule nucleation into asters.

Inhibition of spindle assembly by the mutant transportin TLB is rescued by the potent NLS M9M but not by RanGTP

To address transportin's mechanism of action from a different direction, we performed spindle assembly in the presence of a mutant form of transportin, referred to as truncated-loop karyopherin β2 (TLB). TLB was previously constructed to have a deletion of the H8 loop (Chook *et al.*, 2002). TLB binds both cargo and RanGTP with similar affinities as wild-type transportin, but because the H8 loop has been deleted, the binding of RanGTP does not displace bound cargo (Figure 1B, lower right). Nuclei were formed in *Xenopus* interphase egg extract and the DNA allowed to replicate. An aliquot of mitotic extract was then added to convert the system to a mitotic state, together with added rhodamine-labeled tubulin. Five minutes later, upon verification of mitotic conversion, we added different recombinant proteins and assessed the resulting microtubule structures 1 h later. When control proteins GST or MBP were added, ~80% of the structures observed around chromatin were strong bipolar spindles (Figure 4, A and B; quantitated in Figure 4I, bipolar spindles, gray and dark green bars). Addition of excess wild-type transportin prevented spindle assembly around condensed chromatin, as we observed previously (Lau *et al.*, 2009; Figure 4, C and I, no microtubules, yellow bar). Notably, addition of the mutant transportin TLB also prevented spindle assembly (Figure 4, D and I, no microtubules, red bar).

Addition of RanGTP with wild-type transportin rescued spindle assembly (10 and 20 µM, respectively), with 55% of the condensed chromatin packages showing strong bipolar spindles (Figure 4, E and I, bipolar spindles, purple bar; see also Lau *et al.*, 2009). However, the addition of RanGTP with the mutant transportin TLB (10 and 20 µM) did not rescue spindle assembly. The great major-

ity of condensed chromatin packages (≥95%) had no associated microtubules at all (Figure 4, F and I, no microtubules, dark blue bar). It is important to note that the 10 µM RanGTP concentration was chosen because 15–20 µM RanGTP addition was so potent that asters formed everywhere in the reaction and normal spindle formation was rare (unpublished data); this is presumably due to such a large-scale release of SAFs that microtubule nucleation occurs everywhere, not only around chromatin.

Indeed, the most illustrative addition proved to be that of M9M to either form of transportin. M9M binds both transportin and TLB with extremely high affinity to release bound cargoes from both proteins (Chook *et al.*, 2002; Cansizoglu *et al.*, 2007). The addition of M9M (10 µM) together with excess transportin (20 µM) was able to rescue spindle assembly; > 65% of the condensed chromatin was now present in strong bipolar spindles (Figure 4, G and I, bipolar spindles, light green bar). Most tellingly, M9M (10 µM) also rescued inhibition by TLB (20 µM). Greater than 70% of the condensed chromatin was in strong bipolar spindles (Figure 4, H and I, bipolar spindles, pink bar). The reversal of TLB inhibition by M9M strongly implies that the recovery of spindles around condensed chromatin had to be caused by M9M reversing TLB's sequestration of specific SAFs.

TLB and M9M support a direct inhibition model for transportin in nuclear membrane assembly

Transportin and importin β negatively regulate nuclear membrane assembly by blocking necessary membrane fusion, such that the assembly never progresses beyond membrane vesicle binding. Inhibition is prevented by the inclusion of RanGTP, such that RanGTP promotes vesicle fusion and formation of a continuous nuclear envelope (Zhang *et al.*, 1999, 2002a,b; Clarke and Zhang, 2004; Hetzer *et al.*, 2002; Harel *et al.*, 2003a; Walther *et al.*, 2003b; Lau *et al.*, 2009). However, the mechanism by which transportin negatively regulates nuclear membrane assembly has been unknown. Does transportin act by titrating RanGTP, thus limiting its ability to counteract importin β, or does transportin act more directly by masking factors needed for nuclear membrane vesicle fusion and formation?

To address this, we performed an in vitro nuclear membrane assembly assay in conjunction with the M9M and TLB tools used earlier. To initiate nuclear assembly, we added sperm chromatin and membranes to high-speed interphase egg cytosol. Under control conditions, complete fusion was observed, leading to the presence of fused nuclear membranes around the chromatin, as shown by a smooth, continuous membrane-staining pattern (CTL, Figure 5A, green). Fusion was also observed when RanQ69LGTP (+Ran, Figure 5D) or 1,2-bis(2-aminophenoxy)ethane-*N,N,N,N* tetraacetic acid (BAPTA) was added to the reaction (+BAPTA, Figure 5B). BAPTA, a Ca^{2+} chelator, allows nuclear membrane assembly around DNA but prevents nuclear pore formation (Macaulay and Forbes, 1996), whereas RanQ69L-GTP promotes extensive nuclear membrane fusion and nuclear pore formation (Harel *et al.*, 2003a; Lau *et al.*, 2009). As a negative control for lack of fusion, 2 mM GTPγS was added, which prevents vesicle–vesicle fusion, as indicated by a discontinuous membrane appearance (Newport and Dunphy (1992; +GTPγS, Figure 5C). Addition of transportin also blocked vesicle–vesicle fusion, as seen from the discontinuous green stain (+TRN, Figure 5E), and this inhibition was reversed by RanQ69L-GTP (+TRN+Ran, Figure 5F; Lau *et al.*, 2009).

Strikingly, the addition of the super-NLS M9M prevented transportin's block of nuclear membrane assembly (+TRN+M9M, Figure 5G). When the transportin mutant TLB was added, we found that, like transportin, it blocked nuclear membrane assembly; a discontinuous membrane stain was observed (+TLB, Figure 5H).
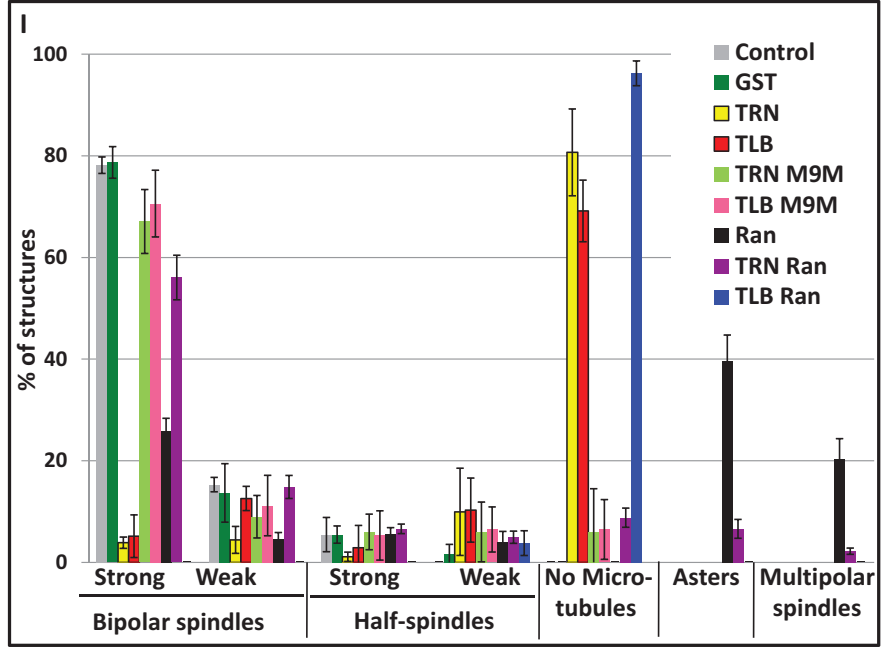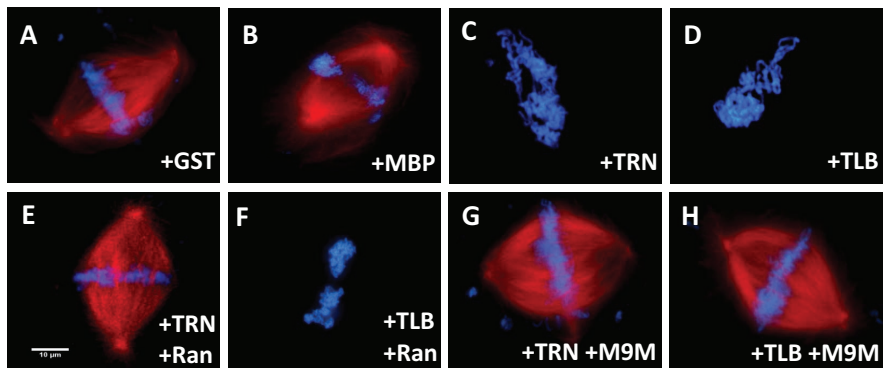
FIGURE 4: TLB inhibition of spindle assembly can be reversed by M9M addition but not by RanGTP addition. (A–H) Interphase *Xenopus* egg extract was mixed with sperm chromatin and rhodamine-labeled tubulin; nuclei were allowed to form, and the DNA was allowed to replicate for 1 h. A portion of this reaction was added to mitotic *Xenopus* extract to convert it to a mitotic state. Recombinant proteins were added as noted and the resulting structures examined by immunofluorescence microscopy; microtubules are red and chromatin is blue due to Hoechst DNA dye. Representative images. (A, B) Here 20 μM GST and 10 μM MBP are controls and show normal bipolar spindles. (C, D) Addition of 20 μM GST-transportin or 20 μM GST-TLB produced almost no microtubule formation over chromatin. (E) As shown in Lau *et al.* (2009), 10 μM RanQ69L-GTP plus 20 μM GST-transportin induced rescue of normal bipolar spindle assembly. (F) Use of 10 μM RanQ69L-GTP plus 20 μM GST-TLB produced essentially no microtubule formation over chromatin. (G) Use of 10 μM MBP-M9M plus 20 μM GST-transportin gave robust bipolar spindle assembly. (H) Use of 10 μM MBP-M9M plus 20 μM GST-TLB also produced robust bipolar spindle assembly. (I) Quantitation of the effects of addition of TLB, transportin, M9M, and RanGTP on spindle assembly. Five replicates of the experiment in A–H were done. Coverslips from each condition were examined and the different structures quantified; ~150 structures were examined for each condition in each experiment. Analysis of the combined results are shown in the graph. As shown by the error bars, little variability was observed between the five different experiments. Control conditions (10 μM MBP or 20 μM GST; gray, green bars) showed almost 80% normal bipolar spindles. Addition of 20 μM GST-TLB or 20 μM GST-transportin to the reaction caused dramatic loss of spindle formation, down to 5% or less in these experimental conditions (yellow, red bars). Addition of 10 μM RanQ69L-GTP with 20 μM GST-transportin (purple bar) rescued this inhibition to ~55% normal spindles. However, addition of 10 μM RanQ69L-GTP to the 20 μM GST-TLB condition showed no increase in spindle formation (blue bar; <5% normal bipolar spindles). Surprisingly, addition of 10 μM MBP-M9M to 20 μM GST-transportin (light green) rescued normal bipolar spindles >65%. Addition of 10 μM MBP-M9M to 20 μM GST-TLB pink bar) was also rescued to >70% normal bipolar spindles.

However, unlike the case of transportin, RanQ69L-GTP could not rescue TLB inhibition of membrane assembly (+TLB+Ran, Figure 5I). In contrast, M9M efficiently counteracted TLB inhibition, allowing nuclear membrane assembly (+TLB+M9M, Figure 5J).

To verify the aforementioned fusion, we tested the *permeability* of the nuclear envelopes formed in each condition using 70-kDa rhodamine-labeled dextran, which cannot pass through fully fused nuclear envelopes (whether or not they have functional nuclear pores; Lau *et al.*, 2009). In all conditions in which vesicle–vesicle fusion was inhibited (+ GTPγS, +TRN, +TLB, or +TLB+Ran), the membranes surrounding the chromatin were indeed permeable to 70-kDa rhodamine-labeled dextran, such that the panels were evenly red in appearance (Figure 5, C, E, H, and I, red). In contrast, in all the conditions in which the membrane stain had indicated the nuclei possessed fully fused nuclear envelopes (CTL, +BAPTA, +TRN+Ran, +TRN+M9M, +TLB+M9M), the nuclei were impermeable to 70-kDa rhodamine-labeled dextran (black holes in red backgrounds, Figure 5, A, B, D, F, G, and J). We conclude that transportin regulates nuclear membrane assembly, not through Ran competition, but through a direct mechanism that can be reversed by M9M.

TLB and M9M confirm a direct inhibition model for transportin in nuclear pore assembly

The nuclear pore complexes consist of ~30 different Nups in multiple copies (Reichelt *et al.*, 1990; Hinshaw *et al.*, 1992; Allen *et al.*, 2000; Rout *et al.*, 2000; Cronshaw *et al.*, 2002; Lim *et al.*, 2008). In higher organisms, the nuclear pores disassemble into ~13 subunits at mitotic entry. There are two times in the cell cycle when nuclear pores assemble from their subunits: 1) in interphase, when pore number doubles to provide for future division, and 2) in telophase, when all the pores that were disassembled in prophase need to reassemble in the two new daughter nuclei. It is the telophase assembly that transportin is known to negatively regulate. Excess transportin addition prevents nuclear pore assembly independently of nuclear membrane assembly. RanGTP counteracts this negative regulation (Lau *et al.*, 2009). Nuclear pore assembly can be isolated and studied as a step independent of nuclear membrane assembly by performing assembly in the presence of the calcium chelator BAPTA. The resulting pore-free
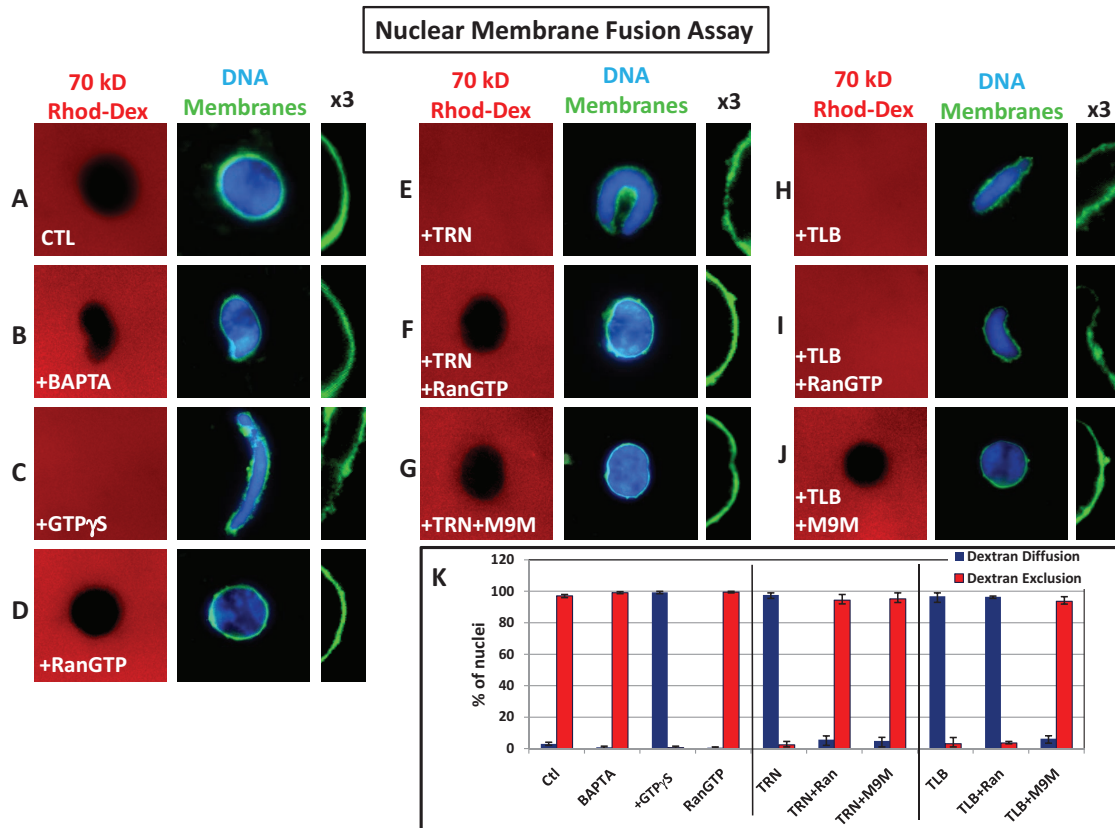
FIGURE 5: Transportin inhibition of nuclear membrane fusion is rescued by M9M addition. (A–H) High-speed interphase *Xenopus* egg extract was mixed with sperm chromatin and membranes and allowed to incubate at room temperature for 60 min. Recombinant proteins were added at the concentrations detailed in *Materials and Methods*. The resulting nuclear structures were examined for integrity using 70-kDa rhodamine–dextran exclusion and for membrane fusion with the membrane dye DHCC (green). Chromatin was stained with Hoechst DNA stain (blue). (A) As a control, addition of 15 μM GST showed smooth nuclear envelope staining and impermeability to 70-kDa dextran. (B, D) The same phenotype was observed when 8 mM BAPTA or 15 μM RanQ69L-GTP was added to the reaction. (C) Addition of 2 mM GTPγS prevented vesicle–vesicle fusion, shown by the rough nuclear envelope staining around the DNA and a permeable nuclear envelope. (E) Addition of 15 μM GST-TRN prevented vesicle–vesicle fusion, inducing a permeable nuclear envelope. (F, G) Addition of 15 μM RanQ69L-GTP or 15 μM MBP-M9M to 15 μM GST-TRN rescued membrane integrity and continuous envelope staining. (H) Vesicle–vesicle fusion was also inhibited by 15 μM GST-TLB. (I) Addition of 15 μM RanQ69L-GTP could not rescue inhibition by 15 μM GST-TLB. (J) Addition of 15 μM MBP-M9M was able to restore the integrity of the nuclear envelope when added with 15 μM GST-TLB. (K) Quantitation of five different experiments; between 70 and 100 nuclei were examined for each condition for each experiment. Little variability was observed between the five experiments for each condition (±1–5%). Blue bars, percentage of nuclei showing dextran diffusion; red bars, percentage of nuclei excluding dextran; representative images in A–J.

nuclear membrane–enclosed intermediates (Figure 6A) can then be diluted into fresh interphase cytosol plus or minus specific inhibitory proteins in order to assess the effect of those proteins on the nuclear pore assembly step (Macaulay and Forbes, 1996; Harel *et al.*, 2003a; Delmar *et al.*, 2008). To examine nuclear pore assembly, we generated BAPTA pore-free nuclear intermediates containing fully fused nuclear membranes (Figure 6A). When such intermediates were diluted 1:10 into fresh *Xenopus* egg cytosol plus the control protein MBP, nuclear pore assembly occurred (+MBP, Figure 6B, red). This rescue of normal pore assembly was apparent from the appearance of punctuate FG nucleoporin staining on the nuclear rim, as depicted in the +MBP control condition.

Addition of transportin completely inhibited the incorporation of FG-nucleoporins into the nuclear envelopes of the pore-free intermediates (+TRN, Figure 6C). As in the case of spindle assembly and nuclear membrane formation, addition of RanGTP rescued the block

to nuclear pore assembly by transportin (+TRN+Ran, Figure 6D). Of note, whereas the transportin mutant TLB also blocked nuclear pore assembly (+TLB, Figure 6F), the addition of RanGTP did *not* reverse the block to pore assembly (+TLB+Ran, Figure 6G). Strikingly, however, addition of the super-NLS M9M with either transportin or the mutant transportin TLB rescued nuclear pore assembly (+TRN+M9M, Figure 6E; +TLB+M9M, Figure 6H). These results strongly support transportin acting as a negative regulator of nuclear pore assembly not by Ran sequestration, but instead by direct inhibition of proteins involved in NPC assembly.

Transportin binds a subset of nucleoporins in mitosis in an M9M-sensitive manner

The foregoing evidence indicates that transportin negatively regulates multiple mitotic assembly events by "assembly factor" binding. When considering potential targets, we examined what is already known about transportin's known nucleoporin binding
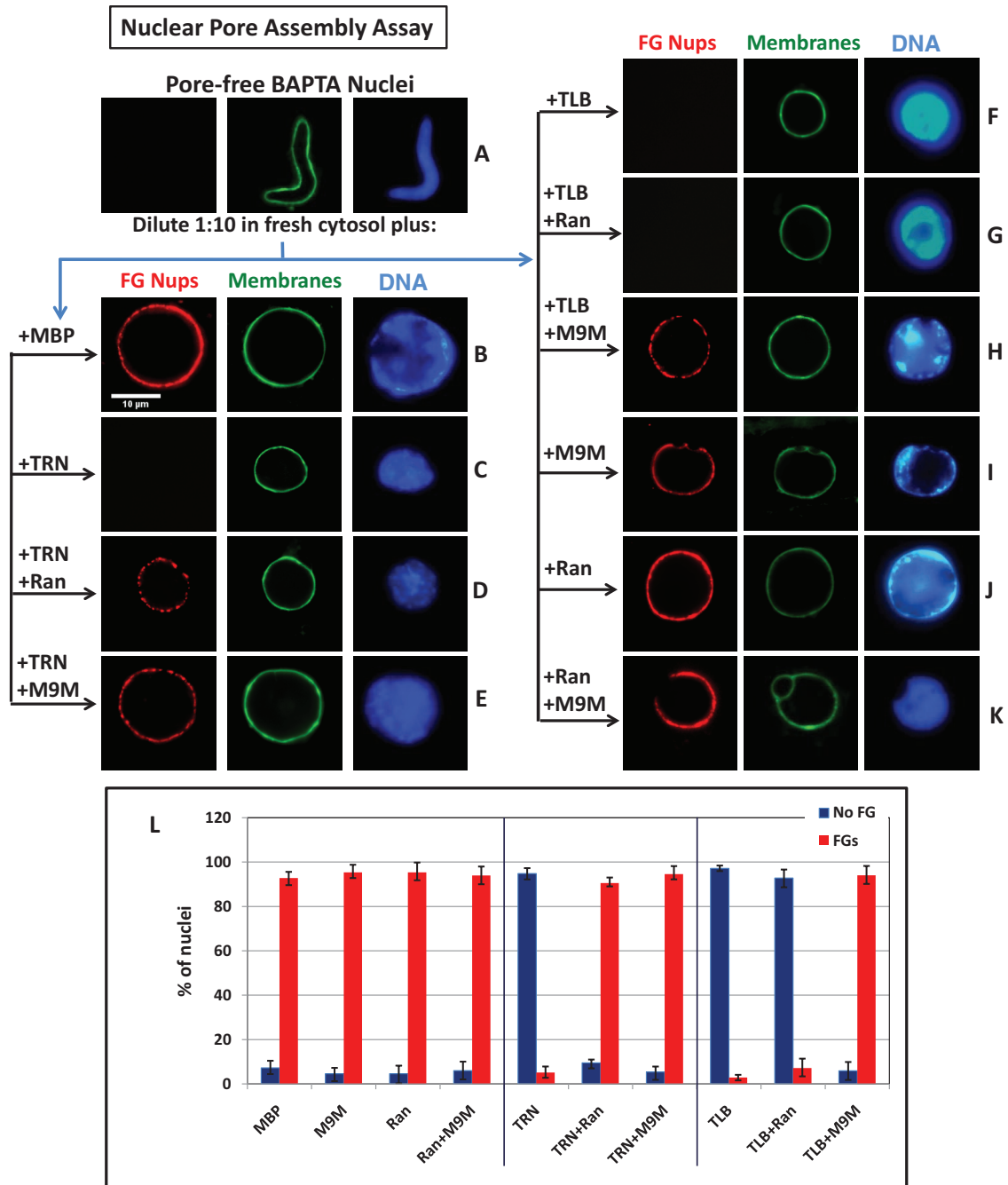
FIGURE 6: Nuclear pore assembly inhibition by excess transportin is reversed by M9M. (A) To assemble pore-free nuclear intermediates, we incubated sperm chromatin, interphase egg extract, and membranes in the presence of 8 mM BAPTA for 60 min. Pore-free nuclei containing fused nuclear membranes were formed (Macaulay and Forbes, 1996). Nuclear pore assembly was tested under different conditions by diluting an aliquot of these pore-free nuclei 1:10 into fresh cytosol and incubating for another 60 min. The presence of nuclear pores was detected by staining for FG-nucleoporins (mAb414-Alexa555; red), whereas membranes were stained with DHCC (green) and the DNA with Hoechst dye (blue). (B) Addition of 15 µM MBP as a control allowed nuclear pore assembly; red. (C) Addition of 15 µM GST-TRN inhibited nuclear pore assembly. (D, E) Addition of 15 µM RanQ69L-GTP or 15 µM MBP-M9M with 15 µM GST-TRN rescued nuclear pore assembly. (F) The presence of 15 µM GST-TLB abolished nuclear pore assembly. (G) Addition of 15 µM RanQ69L-GTP with GST-TLB did not rescue nuclear pore assembly; however, (H) addition of 15 µM MBP-M9M to 15 µM GST-TLB did rescue nuclear pore assembly. (I–K) As controls, we found that the addition of 15 µM MBP-M9M, 15 µM RanQ69L-GTP, or a combination of both did not interfere with nuclear pore assembly. (L) Quantitation of five different experiments; between 70 and 100 nuclei were examined for each condition for each experiment. Little variability was observed between experiments within a condition (±1–6%). Only two types of results were observed: blue bars indicate the percentage of nuclei without FG Nups, and red bars indicate the percentage of nuclei with abundant FG-containing nuclear pores. Representative images in A–K.
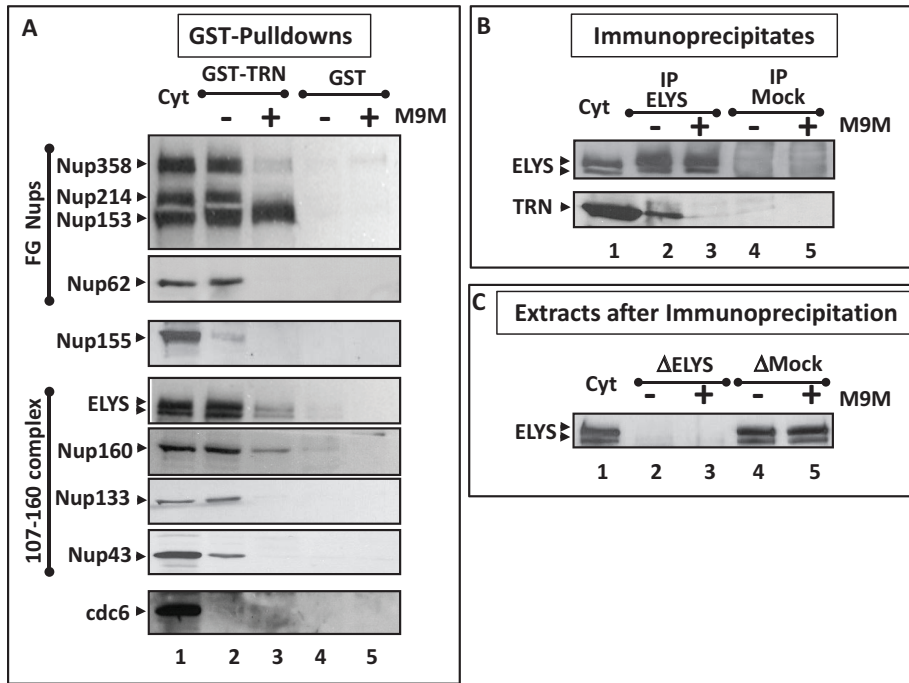
FIGURE 7: Multiple FG nucleoporins and the Nup107–160 complex are transportin-binding targets that are released by M9M. (A) GST or GST-transportin beads were incubated with *Xenopus mitotic* cytosol for 1 h at room temperature. The bound proteins were analyzed by immunoblotting. An aliquot of mitotic cytosol is shown in lane 1 (Cyt). FG-nucleoporins (Nup358, Nup214, Nup153, and Nup62), members of the Nup107–160 complex (Nup160, Nup133, and Nup43), and ELYS were seen to interact with transportin (GST-TRN; lane 2; Lau *et al.*, 2009). Neither Nup155 nor the non-Nup cdc6 protein, tested as a negative control, associated with transportin (GST-TRN; lane 2). GST-bound beads did not interact with any of the tested nucleoporins (GST; lane 4). When M9M was added in the reaction in lane 3 (GST-TRN+M9M), only Nup153 remained bound to the beads. (B) To determine whether the interaction of endogenous *Xenopus* ELYS with endogenous transportin was sensitive to M9M, immunoprecipitation from mitotic *Xenopus* egg extract was performed using anti-xELYS antibodies. This was followed by immunoblotting with anti-ELYS or anti-transportin. Immunoprecipitation of ELYS (lane 2, top) shows that transportin coimmunoprecipitates (lane 2, bottom). Lane 3 shows that addition of M9M to the extract prevents ELYS from binding to transportin. Neither ELYS nor TRN is present in mock immunoprecipitations using control immunoglobulin G (IgG) plus and minus M9M (lanes 4 and 5). (C) The anti-ELYS antiserum is specific. The ELYS doublet was present in mitotic extract mock depleted with IgG beads (ΔMOCK; lanes 4 and 5) but was absent from mitotic cytosol previously subjected to immunodepletion of ELYS (ΔELYS; lanes 2 and 3).

partners. Minimally, these include import cargoes and nucleoporins. In interphase, a transportin–cargo complex has to bind FG-nucleoporins as the import complex passes through the intact nuclear pore (Powers *et al.*, 1997; Bayliss *et al.*, 2000c; Chook and Blobel, 2001; Chook and Suel, 2011; Blevins *et al.*, 2003; Fried and Kutay, 2003; Mosammaparast and Pemberton, 2004; Strawn *et al.*, 2004; Frey *et al.*, 2006; Walde and Kehlenbach, 2010). In addition, we have demonstrated biochemically that transportin binds to a subset of nucleoporins in a Ran-regulated manner (Lau *et al.*, 2009). These include not only FG-nucleoporins, but also the scaffold nucleoporins of the large Nup107–160 complex and its associated partner ELYS (Harel *et al.*, 2003b; Walther *et al.*, 2003a; Loiodice *et al.*, 2004; Galy *et al.*, 2006; Orjalo *et al.*, 2006; Rasala *et al.*, 2006; Franz *et al.*, 2007; Boehmer *et al.*, 2008; Mishra *et al.*, 2010; Bilokapic and Schwartz, 2012, 2013). However, we did not know whether these nucleoporins were interacting with transportin via its cargo-binding site or through a different binding site. To address this, we performed GST pull downs from *Xenopus* mitotic

cytosol using GST or GST-transportin, in the presence or absence of M9M.

We found that in *mitotic* cytosol, GST-transportin binds to the FG nucleoporins Nup358, Nup214, Nup153, and Nup62. Strikingly, addition of M9M prevented this interaction, except in the case of Nup153 (Figure 7A, FG-Nups, compare lanes 2 and 3). We also found that transportin bound to the major scaffold subunit of the pore, the Nup 107–160 complex and its binding partner ELYS. This binding to transportin in mitotic extract was lost upon M9M addition (Figure 7A, 107–160 complex, compare lanes 2 and 3). We further noted that the same Nups and Nup subcomplexes bind to transportin in *Xenopus* egg *interphase* cytosol and that those interactions too are disrupted by M9M (unpublished data).

Not all nucleoporin subunits bind to transportin: Nup155, a member of a different pore scaffold subunit, did not bind, indicating that this subunit is not a target of transportin (Figure 7A, Nup155, lanes 2 and 3). As another negative control, we tested the non-Nup protein cdc6, a member of the DNA prereplicative complex, for interaction with transportin. Cdc6 is carried into the nucleus via importin α/β in *Saccharomyces cerevisiae* (Hahn *et al.*, 2008) and, consistent with this, we found that cdc6 did not interact with transportin (Figure 7A, cdc6).

To test whether the endogenous protein ELYS is normally found bound to endogenous transportin in mitotic *Xenopus* egg extracts, we immunoprecipitated ELYS and probed the immunoprecipitate with anti-transportin antibodies. We found that endogenous ELYS and transportin do coimmunoprecipitate (Figure 7B, lane 2, ELYS and TRN) and that this interaction is abolished by M9M addition to the *Xenopus* mitotic cytosol used for the immunoprecipitation (Figure 7B, compare lanes 2 and 3,

TRN). As a control, we showed that M9M does not interfere in any way with the antibody immunoprecipitation of ELYS itself, since ELYS can be completely depleted from mitotic extract even in the presence of M9M (Figure 7C, lane 3, ΔELYS). Together these results strongly demonstrate that transportin binds to a subset of potential targets, such as specific nucleoporin subunits in their disassembled mitotic state. This is consistent with transportin preventing pore subunit assembly in membranes that are distant from chromatin.

Transportin regulates kinetochore binding of the Nup107–160 complex and ELYS nucleoporins

Next we tested whether the addition of excess transportin blocks Nup107–160 complex recruitment to kinetochores during mitosis in vitro. Of importance, it is known that a pool of the Nup107–160 complex and ELYS localizes to the kinetochores during metaphase in both mammalian cells and *Xenopus* egg extracts (Belgareh *et al.*, 2001; Loiodice *et al.*, 2004; Galy *et al.*, 2006; Orjalo *et al.*, 2006; Rasala *et al.*, 2006; Franz *et al.*, 2007; Zuccolo *et al.*, 2007; Mishra

Kinetochore assay

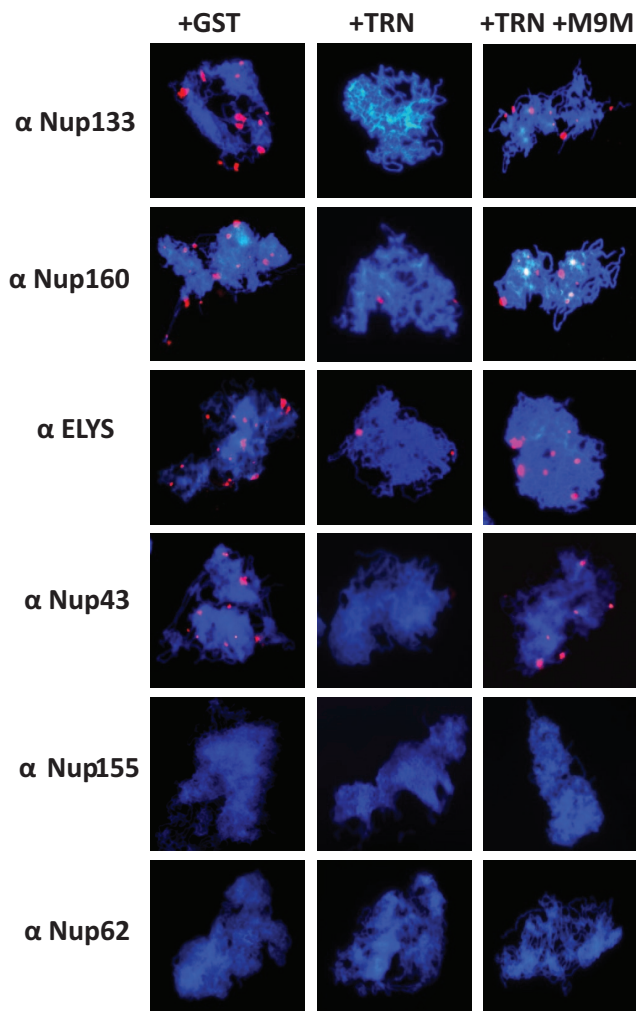|	+GST	+TRN	+TRN +M9M
α Nup133			
α Nup160			
α ELYS			
α Nup43			
α Nup155			
α Nup62			

FIGURE 8: Transportin regulates kinetochore binding of ELYS and the Nup107–160 complex. Mitotic *Xenopus* egg extract was mixed with sperm chromatin, and the chromatin was allowed to remodel and condense for 60 min. Where indicated, GST-transportin (+TRN) or GST-transportin plus MBP-M9M (TRN+M9M) was added at 20 μM at t = 0 min. The presence of nucleoporins on kinetochores was detected by immunofluorescence with Nup-specific antibodies (red dots). In control conditions (+GST), nucleoporins of the Nup107–160 complex and ELYS each showed a dot-like staining on kinetochores (αNup133, αNup160, αELYS, αNup43), as expected (Belgareh et al., 2001; Orjalo et al., 2006; Rasala et al., 2006). Addition of GST-transportin (+TRN; 20 μM) caused almost-complete disappearance of the nucleoporin staining on kinetochores (αNup133, αNup160, αNup43, αELYS). However, inclusion of 20 μM MBP-M9M with 20 μM GST-transportin (+TRN+M9M) restored the kinetochore localization of these particular Nups. Antibodies to the nucleoporins Nup155 and Nup62 did not show any staining on kinetochores under any condition (as previously shown; Orjalo et al., 2006), serving as a negative control. This experiment was performed three times; ~70 mitotic chromosome packages were observed per condition. Representative images are shown for each condition and antibody probe.

et al., 2010). Moreover, this localization to the outer kinetochore region is critical for mitotic spindle assembly and kinetochore function. For example, mitotic extracts depleted of the Nup107–160

complex cannot form a mitotic spindle (Orjalo et al., 2006). We added sperm chromatin to *Xenopus* mitotic egg extracts supplemented with GST, transportin (20 μM), or transportin plus M9M (20 μM+20 μM). We tested the recruitment of the Nup107–160 complex and other nucleoporins to kinetochores on the resulting condensed chromatin by immunofluorescence (Orjalo et al., 2006). When the control protein GST was added, Nup133, Nup160, and Nup43 showed kinetochore localization (Figure 8, +GST). The same kinetochore localization was found for ELYS (αELYS, +GST). As a negative control, we analyzed Nup155 and Nup62, which are known not to be localized at kinetochores during mitosis (Orjalo et al., 2006), and observed no such presence (Figure 8, +GST, αNup155, and αNup62). Addition of 20 μM GST-transportin to the assay greatly reduced the presence of Nup133, Nup160, Nup43, and ELYS on chromatin (Figure 8, +TRN). However, addition of GST-transportin with MBP-M9M (20 μM each) restored Nup107–160 complex and ELYS localization to chromatin (Figure 8, +TRN+M9M). These results are consistent with transportin being able to regulate the kinetochore localization of the Nup107–160 nucleoporins.

DISCUSSION

Transportin negatively regulates three major mitotic assembly events: spindle assembly, nuclear membrane assembly, and nuclear pore assembly (Lau et al., 2009). To probe mechanisms of action, we took advantage of the synthetic NLS-peptide M9M, which has been shown to be a potent transportin inhibitor of nuclear import in human cells (Cansizoglu et al., 2007). We determined that M9M interacts specifically with both recombinant and endogenous *Xenopus* transportin but not with importin β (Supplemental Figure S1). Upon examination, M9M-transfected HeLa cells showed striking defects, including an increased number of cells with microtubule midbodies, DNA bridges, and multiple nuclei. In those cells that were in metaphase, the great majority showed abnormal spindles. Indeed, almost 30% of all M9M-transfected cells showed a defect in either completion of cytokinesis or spindle assembly (Figure 2). Thus inhibition of transportin clearly results in significant mitotic defects in vivo. Switching to an in vitro approach allowed us specifically to study the effect of inhibiting transportin on the mitotic spindle. We found that addition of M9M to spindle assembly extracts containing chromatin produced not only larger bipolar spindles, but also giant spindles, multipolar spindles, and free asters (Figure 3B). Strikingly, even in chromatin-minus conditions, M9M induced aster assembly (Figure 3, E–G).

Previous studies revealed that the addition of excess RanGTP to *Xenopus* mitotic extracts caused the release of specific spindle assembly factors from a strong masking inhibition by importin β or importin α/β (Carazo-Salas et al., 1999; Kalab et al., 1999; Ohba et al., 1999; Wilde and Zheng, 1999; Zhang et al., 1999; Clarke and Zhang, 2008; Gruss et al., 2001; Nachury et al., 2001; Di Fiore et al., 2004; Ribbeck et al., 2006; Lau et al., 2009; Cross and Powers, 2011). Moreover, when this increased unmasking by excess RanGTP occurred in the vicinity of chromatin, the spindles produced were larger than normal because spindle size was no longer limited by the reach of the RanGTP created only by chromatin-bound RCC1 (Bischoff and Ponstingl, 1991a,b; Clarke and Zhang, 2008; Kalab and Heald, 2008).

If transportin binds and inhibits SAFs, then the addition of M9M might well induce the same microtubule structures induced by excess RanGTP. This was what we saw (Figure 3, B and C). Indeed, with a direct target inhibition model, in which transportin binds to and regulates spindle assembly factors, either RanGTP or M9M addition should free SAFs. RanGTP would do so by

releasing the cargo SAFs via an H8-loop allosteric mechanism. M9M would do so by binding to the cargo site of transportin with extreme affinity and thus displacing the cargo SAFs. In both cases, the freed SAFs would then be available to induce larger spindles than normal, as well as free asters. Would there be any difference expected between RanGTP and M9M observed phenotypes? Because RanGTP would free both transportin- and importin β–bound SAFs, whereas M9M would free only transportin-bound SAFs, the excess RanGTP condition would be expected to show more and larger asters, as well as slightly larger spindles than the M9M condition. This was what we found (Figure 3, B, C, and E–G). Thus we conclude that the M9M results support a direct target inhibition mechanism for transportin action.

Another route to determining the mechanism by which transportin regulates mitotic events was to use the mutant transportin, TLB. Ran binding and cargo binding are uncoupled in TLB, such that the mutant TLB transportin fails to undergo cargo release upon Ran binding. The mutant still binds RanGTP in its N-terminal domain, but this does not release bound cargo from the C-terminal domain (Chook *et al.*, 2002). We found that addition of TLB strongly inhibited spindle assembly in vitro, just as transportin does (Figure 4, C and D). However, unlike transportin, TLB inhibition was not reversed by RanGTP (Figure 4F). If transportin regulates through a mechanism by which it *depletes* RanGTP, then TLB should also still deplete RanGTP, and TLB's inhibitory activity should be reversed by providing the same amount of RanGTP that reverses transportin inhibition. Because this did not occur, the TLB results independently point toward a direct target model.

The most definitive evidence for direct target inhibition, however, came from the addition of M9M in combination with TLB. Adding M9M with TLB caused robust rescue of spindle assembly (Figure 4H). This means that M9M, when binding with high affinity to the cargo site of transportin, must be releasing one or more factors that restore spindle assembly. Put another way, rescue of spindle assembly by M9M must be due to M9M keeping TLB from binding and inhibiting spindle assembly factors in its cargo site. Thus we conclude that transportin acts during spindle assembly by masking spindle assembly factors.

Evidence supporting a direct inhibition mechanism for transportin in both nuclear membrane assembly and nuclear pore assembly was similarly found. RanGTP could not rescue TLB inhibition of nuclear membrane or nuclear pore assembly, but M9M could (Figures 5 and 6). The targets inhibited by transportin for nuclear membrane assembly are unknown, but here we show that in *mitotic* extracts, multiple nuclear pore proteins bind to transportin and do so in an M9M-reversible manner (Figure 7). Transportin does not bind to all Nups. For example, it fails to bind to the pore scaffold component Nup155 (Figure 7; Lau *et al.*, 2009). However, of those Nups that transportin does bind, with the exception of Nup153, all show M9M-reversible binding. This includes the FG nucleoporins Nup358, Nup214, and Nup62, the Nup107–160 complex (as tested with anti-Nup160, -Nup133, and -Nup43 antibodies), and the pore-targeting protein ELYS. In consequence, the data strongly suggest that transportin regulates the nuclear pore assembly event that occurs in late mitosis by *directly* binding and inhibiting multiple soluble nuclear pore proteins needed for pore assembly everywhere except in the vicinity of chromatin.

On the basis of these data, one can speculate that in *mitosis* the aforementioned nucleoporins bind to transportin in its cargo-binding site and are displaced from the site by M9M. If true, this would mean that the Nups bind to transportin in mitosis via a *different* transportin-binding site than they do in interphase. Of note, importin
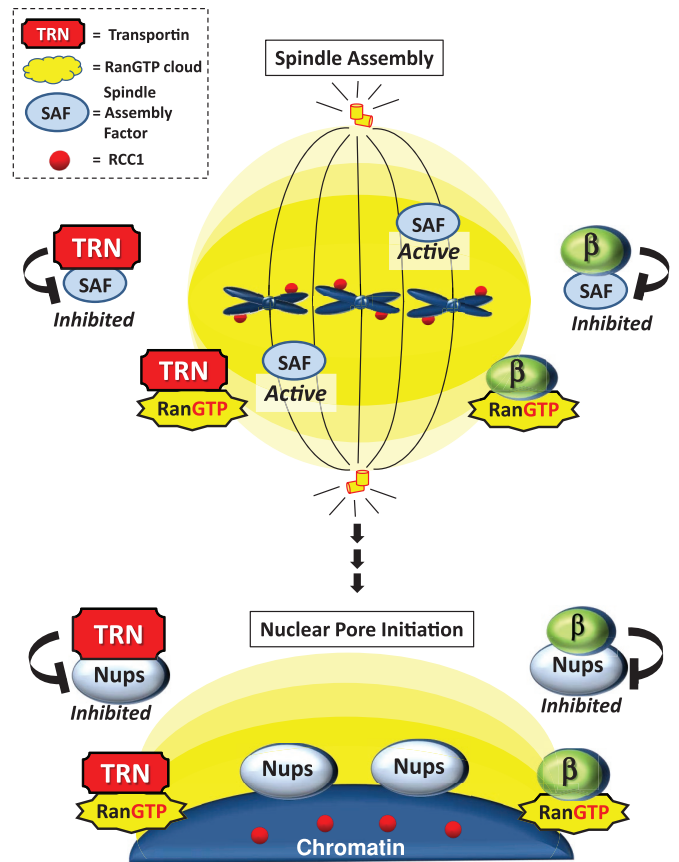

FIGURE 9: Mechanistically parallel transportin and importin β GPS pathways. As depicted in the model shown, transportin (TRN) acts by a mechanism parallel to that of importin β, that is, by direct factor inhibition. Spindle assembly at metaphase requires spindle assembly factors or SAFs (blue spheres; top half). As the cell cycle proceeds, a subsequent mitotic assembly event that occurs is the initiation of nuclear pore assembly in telophase. This is characterized by the recruitment and binding of an early set of Nups, the Nup107–160 complex and ELYS, to the surface of the decondensing chromatin (Nups; gray-blue spheres; bottom half). In metaphase, transportin mechanistically acts by binding to and inhibiting spindle assembly factors in regions far from the chromatin; in contrast, SAFs near chromatin are released from transportin by the RanGTP cloud (yellow), produced by the chromatin-bound RanGEF RCC1 (small red spheres), and release promotes spindle assembly. Later, after the spindle has disassembled and telophase begins, nucleoporins such as the Nup107–160 complex and ELYS are inhibited by transportin in regions far from chromatin, but those near chromatin are released from transportin by the RanGTP cloud and initiate nuclear pore assembly on the surface of chromatin. Importin β was shown previously to pursue a similar mechanism of inhibition counteracted by localized RanGTP production, which acts as a GPS system to tell where the mitotic assembly events should take place (see text for references). From the data in Figures 3–8, we conclude that transportin and importin β have mechanistically parallel regulatory mechanisms for the major mitotic assembly events. Of importance, not only is the Nup107–160 complex vital for nuclear pore initiation, but it is in fact also a SAF essential to metaphase kinetochore function. Thus, by regulating this one protein complex, transportin can regulate both spindle and nuclear pore assembly.

β does indeed bind to FG nucleoporins during nuclear import using binding sites distinct from its cargo-binding site (Bayliss *et al.*, 2000a,c; Bednenko *et al.*, 2003).

Returning once again to spindle assembly, the spindle has been predicted to contain ~800 proteins (Sauer *et al.*, 2005). Although it would be unlikely that all are needed for the act of spindle assembly, assuredly many are. Importin β has been shown to negatively regulate at least 13 or 14 different SAFs in a Ran-dependent manner (Kalab and Heald, 2008). To seek transportin-regulated SAFs, one could look for PY sequences on known SAFs; however, because of the variablity of the PY-NLS, simple sequence analysis is unlikely to reveal these targets (Suel *et al.*, 2008; Xu *et al.*, 2010). Moreover, a recent study found that transportin also recognizes a second type of NLS signal, the BIB domain, which is LYS-ARG rich and capable of also binding importin β (Kimura *et al.*, 2013). This would make such an undirected approach laborious and of uncertain outcome.

The most meaningful finding, however, is that transportin clearly binds to the Nup107–160 complex and ELYS, both of which localize to kinetochores in mitosis in vivo and in vitro (Belgareh *et al.*, 2001; Loiodice *et al.*, 2004; Galy *et al.*, 2006; Orjalo *et al.*, 2006; Rasala *et al.*, 2006; Franz *et al.*, 2007; Zuccolo *et al.*, 2007; Lau *et al.*, 2009; Mishra *et al.*, 2010). Significantly, the presence of the Nup107–160 complex at kinetochores has been shown to be absolutely essential for spindle assembly; its removal by depletion can cause insurmountable spindle and kinetochore defects (Orjalo *et al.*, 2006; Zuccolo *et al.*, 2007; Mishra *et al.*, 2010). We further show in this study that the Nup107–160 complex and ELYS are demonstrable transportin targets in *mitotic* extracts, since they are found to be bound by transportin and freed by M9M addition (Figure 7). Furthermore, they are prevented from assembling onto mitotic kinetochores by transportin addition in vitro (Figure 8). By showing that these outer kinetochore components are modulated by transportin, we have gone as far toward finding the essence of transportin spindle inhibition as we can without going further back into the inception of the kinetochore, such as searching for a potential transportin inhibition of an inner kinetochore protein.

In conclusion, our data argue that transportin acts directly to bind and mask assembly factors used in spindle assembly, nuclear membrane assembly, and pore assembly to ensure that these structures each assemble only in the vicinity of chromatin (Figure 9). Transportin therefore acts as a "global positioning system" or GPS (Kalab and Heald, 2008) to direct where such structures should assemble. Thus we conclude that the cell contains mechanistically parallel importin β and transportin GPS pathways.

MATERIALS AND METHODS
Antibodies and recombinant proteins
Antibodies used for immunoblotting included mouse anti–human transportin (BD Biosciences, San Jose, CA), anti–*Xenopus* importin β (Delmar *et al.*, 2008), anti–FG Nup mAb414 (Covance, Berkeley, CA), anti-Nup155 (Lau *et al.*, 2009), anti-xELYS (Rasala *et al.*, 2006), anti-Nup160 and anti-Nup133 (Harel *et al.*, 2003b), anti-Nup43 (Orjalo *et al.*, 2006), and anti-cdc6 (Hua and Newport, 1998). For immunofluorescence on HeLa cells, antibodies included a TRITC-labeled anti-myc antibody (Santa Cruz Biotechnology, Santa Cruz, CA) and a FITC-labeled anti-tubulin antibody (DM1A clone, Sigma Aldrich, St. Louis, MO).

GST-human transportin, GST-RanQ69L, and the recombinant form of the transportin mutant TLB, GST-TLB (Chook *et al.*, 2002), were expressed in Rosetta *E. coli* cells from pGEX vectors (Chook *et al.*, 2002; Harel *et al.*, 2003a; Lau *et al.*, 2009). One-liter LB-ampicillin cultures were grown at 37°C until an OD of 0.3–0.6 and induced for 4 h with 1 mM isopropyl-β-ᴅ-thiogalactoside (IPTG).

GST-*Xenopus* importin β was expressed in Rosetta *E. coli* cells from pGEX6P vectors (Delmar *et al.*, 2008). One-liter LB-ampicillin cultures were grown at 37°C until an OD of 0.3, moved to a 16°C water bath, and induced with 0.3 mM IPTG for 4 h and then with 0.7 mM IPTG overnight (~12 h). All GST-tagged proteins were purified on glutathione Sepharose beads (BioWorld, Dublin, OH) per manufacturer's specifications and were eluted from the beads using a glutathione solution (50 mM, pH 7.5). The GST tag was removed from transportin for the quantification studies (Supplemental Figure S1) and from RanQ69L by proteolytic digestion for all experiments using GST-PreScission Protease (GE Healthcare, Piscataway, NJ) overnight at 4°C according to the manufacturer's protocol as described (Lau *et al.* (2009). RanQ69L was loaded with GTP as described (Harel *et al.*, 2003a).

MBP, MBP-M9, and MBP-M9M were expressed in Rosetta *E. coli* cells from pMAL vectors (Cansizoglu *et al.*, 2007). One-liter LB-ampicillin cultures of these were grown at 37°C until an OD of 0.3–0.6 and induced for 4 h with 1 mM IPTG. All MBP-tagged proteins were purified on amylose resin (New England Biolabs, Beverly, MA) according to manufacturer's specifications and eluted with maltose elution buffer (Tris 50 mM, NaCl 50 mM, maltose 50 mM, pH 7.5). These proteins, as well as transportin, importin β, and TLB, were dialyzed into *Xenopus* buffer (XB; 50 mM sucrose, 10 mM 4-(2-hydroxyethyl)-1-piperazineethanesulfonic acid [HEPES], 100 mM KCl, 1 mM $MgCl_2$, 0.1 mM $CaCl_2$) and stored in 5-µl aliquots at –80°C for later use.

HeLa cell transfection
To assess the effect of transportin inhibition on mitosis in vivo (Figure 2), HeLa cells (200,000/well) were seeded in six-well plates containing coverslips (12 mm) and grown overnight 37°C in 5% CO_2. Cells were then transfected using JetPI according to manufacturer's protocol (PolyPlus Transfection, Illkirch, France) with 2 µg of mammalian expression vector pCS2+MT MBP (as a control) or pCS2+MT MBP-M9M (Cansizoglu *et al.*, 2007). The cells were allowed to grow at 37°C and 5% CO_2 for 24 h and then fixed on the coverslips with cold (–20°C) 100% methanol for 20 min and rehydrated with 1× phosphate-buffered saline (PBS) for 1 h. After this, the coverslips were blocked with 5% fetal bovine serum in PBS for 30 min at room temperature and incubated with TRITC-labeled anti-myc and FITC-labeled anti-tubulin antibodies (1:100 dilution in PBS for 1 h at room temperature) before the coverslips were mounted on slides using 2 µl of Vectashield with DAPI mounting media (Vector Labs, Southfield, MI) and visualization with a Zeiss Axioskop 2 microscope and 63× objective. Approximately 200 cells were observed for each condition (MBP or MBP-M9M) and the structures noted and quantified.

Xenopus egg extracts
Newly laid *X. laevis* eggs are naturally arrested in the second metaphase of meiosis by cytostatic factor (CSF; Lohka and Maller, 1985; Sagata *et al.*, 1989; Murray, 1991). This arrested stage is biochemically and physiologically related to a mitotic state. Extracts that are considered either mitotic (CSF) or interphase extracts can easily be generated (Murray, 1991; Chan and Forbes, 2006; Maresca and Heald, 2006; Bernis *et al.*, 2007; Cross and Powers, 2008,). Preparation of the fresh low-speed (crude) mitotic and interphase *Xenopus* egg extracts used for the spindle assay was as described (Lau *et al.*, 2009). For nuclear pore and nuclear membrane assembly assays (see later description), high-speed interphase *Xenopus* egg extracts were prepared as described (Harel *et al.*, 2003a; Chan and Forbes, 2006; Lau *et al.*, 2009).

Xenopus spindle assembly assay

To observe spindle assembly, the protocol used was essentially as in Lau *et al.* (2009). *Xenopus* sperm chromatin was added to *Xenopus* egg interphase extract to allow nuclei to form and the chromatin to replicate. For this, interphase extract was incubated with Energy Mix (10 mM phosphocreatine, 80 µg/ml creatine kinase, 1 mM ATP, 2 mM MgCl$_2$, and 100 mM ethylene glycol tetraacetic acid [EGTA]) and sperm chromatin (70,000 SpC/20-µl interphase extract) at room temperature for 2 h to allow DNA replication. To induce mitosis, 10 µl of this reaction, which now contained nuclei, was mixed with 15 µl of CSF extract, 1 µl of rhodamine-labeled tubulin (Cytoskeleton, Denver, CO), and 2 µl of Energy Mix. On verification of mitotic conversion after 5 min (i.e., visual loss of nuclear membranes, appearance of chromatin condensation and early microtubule structures; as seen in Figure 3, 5-min time point), when indicated, the following proteins were added: 20 µM GST, 10 µM RanQ69L-GTP, 20 µM GST-transportin, 20 µM GST-TLB, 10 µM MBP, or 10 µM MBP-M9M (Figures 3 and 4). The reaction was incubated in the dark at room temperature. At 60 min, 2.5 µl were removed and mounted with 1 µl of fixation buffer (48% glycerol, 11% formaldehyde, 10 mM HEPES, 5 µg/ml Hoechst, pH 7.5) on glass slides. For each condition, between 50 and 100 microtubule structures or condensed chromatin packages were analyzed using a Zeiss Axioskop 2 microscope and a 63× objective (Figures 3 and 4). To measure spindle size (Figure 3D), the surface area of ~40 individual spindles from the conditions MBP, MBP-M9M, and RanQ69L-GTP was measured in three independent experiments using ImageJ software according to the instructions found at http://rsbweb.nih.gov/ij/.

Nuclear membrane fusion and nuclear pore assembly assays

Interphase *Xenopus* high-speed cytosol and membranes and *Xenopus* sperm chromatin were prepared as described (Harel *et al.*, 2003b). The membrane fusion assay (Figure 5) and nuclear pore assembly assay (Figure 6) were performed as described (Harel *et al.*, 2003a). Nuclear membrane assembly was visualized using the fluorescent membrane dye 3,3-dihexyloxacarbocyanine iodide (DHCC; Eastman Kodak, Rochester, NY). Images were processed using ImageJ and Photoshop (Adobe, San Jose, CA). For dextran analysis of membrane integrity, in vitro nuclear reconstitution reactions were carried out as in Harel *et al.* (2003a), except that at the beginning of the reaction, additions were made as follows, where noted: GST as control (15 µM), GTPγS (2 mM), BAPTA (8 mM), RanQ69L-GTP (15 µM), GST-transportin (15 µM), GST-TLB (15 µM), MBP-M9M (15 µM), or combinations thereof. Assembly was allowed to proceed for 45 min, and then wheat germ agglutinin (100 µM; EY Laboratories, San Mateo, CA) was added for 10 min to further ensure a tight seal of any nuclear pores present (although nuclear pores are already expected to exclude 70-kDa dextran; Lau *et al.*, 2009). Reactions were then stopped 5 min on ice, and 1 µl of rhodamine-labeled dextran (70 kDa, 2.5 µg; Molecular Probes, Eugene, OR) was added to a 25-µl reaction, followed by a second incubation for 15 min on ice. The reactions were fixed by dilution 1:1 with egg lysis buffer containing 7.4% paraformaldehyde, and dextran exclusion was visualized.

For nuclear pore assembly, pore-free nuclear intermediates were assembled by adding 8 mM BAPTA (EMD Chemicals, San Diego, CA) to the nuclear formation reaction at $t = 0$ min as described (Macaulay and Forbes, 1996; Harel *et al.*, 2003a). At $t = 60$ min, extract containing BAPTA-arrested pore-free nuclei was diluted 1:10 into fresh cytosol in the presence or absence of recombinant proteins (MBP, MBP-M9M, RanQ69L-GTP, transportin, TLB, or combinations thereof). Reactions were allowed to proceed for additional 60 min. Membranes were visualized with DHCC, and nuclear pore assembly (Figure 6) was visualized by staining for FG nucleoporins with Alexa 555–labeled mAb414 antibody (Covance, Berkeley, CA; Invitrogen, Eugene, OR). For the latter, Alexa 555–mAb414 (1 µg/µl) was diluted 1:50 in the nuclear assembly reaction and allowed to incubate for 15 min before fixation and visualization.

GST pull downs

To assess the M9M sensitivity of nucleoporin interactions with transportin (Figure 7A), magnetic beads containing GST-transportin or GST were prepared. The beads were prepared by incubating 100 µg of GST-transportin or 100 µg of GST with 30 µl of magnetic glutathione beads in 150 µl of 1× PBS for 1 h at room temperature. The protein-coupled beads were then washed twice with 1× PBS and resuspended in 150 µl of PBS. When indicated in Figure 7, 100 µg of MBP-M9M was added and incubated for 1 h at room temperature. The beads were then washed twice with 1× CSF-XB (100 mM KCl, 0.1 mM CaCl$_2$, 1 mM MgCl$_2$, 10 mM HEPES, 50 mM sucrose, and 7 mM EGTA). Each set of beads was then incubated with 50 µl of *Xenopus* mitotic egg extract supplemented with 1× Energy Mix and gently shaken for 1 h at room temperature. The beads were washed two times with RIPA-SDS (50 mM Tris, 150 mM NaCl, 1 mM EDTA, 1% NP40, 1% sodium deoxycholic acid, 1 mM NaF, 1 mM sodium orthovanadate, 1 mM phenylmethylsulfonyl fluoride, pH 7.4), three times with 1× CSF-XB + 0.1% NP40, and two times with 1× CSF-XB before final resuspension in 50 µl of protein sample buffer. Each sample was heated for 5 min at 65°C (to preserve ELYS; Rasala *et al.*, 2006), loaded onto a 5–20% gradient SDS–PAGE gel, and transferred to nitrocellulose. Nucleoporin binding to the protein-coupled magnetic beads was assessed by cutting the blot into strips and immunoblotting with the individual antibodies shown; in some cases of similarly sized nucleoporins, the blot was stripped, verified to be negative, and reprobed with a different antibody. Each type of experiment was performed three to five times.

Determination of ELYS/transportin interaction

To determine whether transportin interacts with endogenous *Xenopus* ELYS protein in an M9M-sensitive manner (Figure 7, B and C), we performed coimmunoprecipitations. Three micrograms of purified anti-xELYS antibody or control immunoglobulin G was incubated with 30 µl of magnetic Protein G beads in 100 µl of 1× CSF-XB for 1 h at room temperature. The beads were then washed twice with 1× CSF-XB. After this, the beads were incubated with 30 µl of *Xenopus* mitotic egg extract at room temperature for 1 h, supplemented where noted with 20 µM M9M. The beads were then washed three times with RIPA-SDS and two times with 1× CSF-XB. The washed beads were resuspended in 40 µl of protein sample buffer and the eluate subjected to gradient 5–20% SDS–PAGE. Immunoprecipitated proteins were analyzed by immunoblotting.

Kinetochore localization of nucleoporins

To analyze mitotic chromatin and kinetochore staining of nucleoporins (Figure 8), 20 µl of *Xenopus* mitotic extract (supplemented with 1× Energy Mix) was incubated with sperm chromatin (70,000 SpC/20-µl mitotic extract) at room temperature as described (Orjalo *et al.*, 2006). Where indicated, 20 µM GST, 20 µM GST-transportin (+TRN), or 20 µM GST-transportin plus 20 µM MBP-M9M (+TRN+M9M) was added at $t = 0$ min. After 60 min of incubation, each reaction was diluted five times in dilution buffer (0.8× XB-EGTA buffer, 250 mM sucrose) and then mixed with 500 µl of a fixation buffer specific to this assay (0.8× XB-EGTA, 250 mM sucrose, 4% formaldehyde) and incubated for 30 min at room temperature (Orjalo *et al.*, 2006). Each reaction was then overlaid onto a glycerol

cushion (40% glycerol, 0.8× XB-EGTA, 0.1% Triton X-100) and spun down onto coverslips for 10 min at 6000 × *g* at 18°C. The coverslips were washed one time with 1× PBS, fixed with −20°C methanol for 30 min, washed twice with 1× PBS, rehydrated with 1× PBS + 0.1% Triton X-100 for 60 min, and blocked with 5% bovine serum albumin in 1× PBS for 60 min. Immunofluorescence assays were performed with anti-nucleoporin antibodies as described (Wood *et al.*, 1997; Arnaoutov and Dasso, 2003; Harel *et al.*, 2003b; Orjalo *et al.*, 2006).

REFERENCES

Aitchison JD, Blobel G, Rout MP (1996). Kap104p: a karyopherin involved in the nuclear transport of messenger RNA binding proteins. Science 274, 624–627.

Allen TD, Cronshaw JM, Bagley S, Kiseleva E, Goldberg MW (2000). The nuclear pore complex: mediator of translocation between nucleus and cytoplasm. J Cell Sci 113, 1651–1659.

Ambrus G, Whitby LR, Singer EL, Trott O, Choi E, Olson AJ, Boger DL, Gerace L (2010). Small molecule peptidomimetic inhibitors of importin alpha/beta mediated nuclear transport. Bioorg Med Chem 18, 7611–7620.

Andrade MA, Bork P (1995). HEAT repeats in the Huntington's disease protein. Nat Genet 11, 115–116.

Arnaoutov A, Dasso M (2003). The Ran GTPase Regulates kinetochore function. Dev Cell 5, 99–111.

Askjaer P, Galy V, Hannak E, Mattaj IW (2002). Ran GTPase cycle and importins alpha and beta are essential for spindle formation and nuclear envelope assembly in living *Caenorhabditis elegans* embryos. Mol Biol Cell 13, 4355–4370.

Bayliss R, Corbett AH, Stewart M (2000a). The molecular mechanism of transport of macromolecules through nuclear pore complexes. Traffic 1, 448–456.

Bayliss R, Kent HM, Corbett AH, Stewart M (2000b). Crystallization and initial x-ray diffraction characterization of complexes of FxFG nucleoporin repeats with nuclear transport factors. J Struct Biol 131, 240–247.

Bayliss R, Littlewood T, Stewart M (2000c). Structural basis for the interaction between FxFG nucleoporin repeats and importin-beta in nuclear trafficking. Cell 102, 99–108.

Bednenko J, Cingolani G, Gerace L (2003). Importin beta contains a COOH-terminal nucleoporin binding region important for nuclear transport. J Cell Biol 162, 391–401.

Belgareh N *et al.* (2001). An evolutionarily conserved NPC subcomplex, which redistributes in part to kinetochores in mammalian cells. J Cell Biol 154, 1147–1160.

Ben-Efraim I, Frosst PD, Gerace L (2009). Karyopherin binding interactions and nuclear import mechanism of nuclear pore complex protein Tpr. BMC Cell Biol 10, 74.

Ben-Efraim I, Gerace L (2001). Gradient of increasing affinity of importin beta for nucleoporins along the pathway of nuclear import. J Cell Biol 152, 411–417.

Bernis C, Vigneron S, Burgess A, Labbe JC, Fesquet D, Castro A, Lorca T (2007). Pin1 stabilizes Emi1 during G2 phase by preventing its association with SCF(betatrcp). EMBO Rep 8, 91–98.

Bilokapic S, Schwartz TU (2012). Molecular basis for Nup37 and ELY5/ELYS recruitment to the nuclear pore complex. Proc Natl Acad Sci USA 109, 15241–15246.

Bilokapic S, Schwartz TU (2013). Structural and functional studies of the 252 kDa nucleoporin ELYS reveal distinct roles for its three tethered domains. Structure 21, 572–580.

Bird SL, Heald R, Weis K (2013). RanGTP and CLASP1 cooperate to position the mitotic spindle. Mol Biol Cell 24, 2506–2514.

Bischoff FR, Gorlich D (1997). RanBP1 is crucial for the release of RanGTP from importin beta-related nuclear transport factors. FEBS Lett 419, 249–254.

Bischoff FR, Klebe C, Kretschmer J, Wittinghofer A, Ponstingl H (1994). RanGAP1 induces GTPase activity of nuclear Ras-related Ran. Proc Natl Acad Sci USA 91, 2587–2591.

Bischoff FR, Ponstingl H (1991a). Catalysis of guanine nucleotide exchange on Ran by the mitotic regulator RCC1. Nature 354, 80–82.

Bischoff FR, Ponstingl H (1991b). Mitotic regulator protein RCC1 is complexed with a nuclear ras-related polypeptide. Proc Natl Acad Sci USA 88, 10830–10834.

Blevins MB, Smith AM, Phillips EM, Powers MA (2003). Complex formation among the RNA export proteins Nup98, Rae1/Gle2, and TAP. J Biol Chem 278, 20979–20988.

Boehmer T, Jeudy S, Berke IC, Schwartz TU (2008). Structural and functional studies of Nup107/Nup133 interaction and its implications for the architecture of the nuclear pore complex. Mol Cell 30, 721–731.

Cansizoglu AE, Chook YM (2007). Conformational heterogeneity of karyopherinβ2 is segmental. Structure 15, 1431–1441.

Cansizoglu AE, Lee BJ, Zhang ZC, Fontoura BM, Chook YM (2007). Structure-based design of a pathway-specific nuclear import inhibitor. Nat Struct Mol Biol 14, 452–454.

Carazo-Salas RE, Guarguaglini G, Gruss OJ, Segref A, Karsenti E, Mattaj IW (1999). Generation of GTP-bound Ran by RCC1 is required for chromatin-induced mitotic spindle formation. Nature 400, 178–181.

Chan RC, Forbes DI (2006). In vitro study of nuclear assembly and nuclear import using *Xenopus* egg extracts. Methods Mol Biol 322, 289–300.

Chook YM, Blobel G (1999). Structure of the nuclear transport complex karyopherin-beta2-Ran x GppNHp. Nature 399, 230–237.

Chook YM, Blobel G (2001). Karyopherins and nuclear import. Curr Opin Struct Biol 11, 703–715.

Chook YM, Jung A, Rosen MK, Blobel G (2002). Uncoupling Kapbeta2 substrate dissociation and ran binding. Biochemistry 41, 6955–6966.

Chook YM, Suel KE (2011). Nuclear import by karyopherin-betas: recognition and inhibition. Biochim Biophys Acta 1813, 1593–1606.

Ciciarello M, Mangiacasale R, Lavia P (2007). Spatial control of mitosis by the GTPase Ran. Cell Mol Life Sci 64, 1891–1914.

Clarke PR, Zhang C (2004). Spatial and temporal control of nuclear envelope assembly by Ran GTPase. Symp Soc Exp Biol 193–204.

Clarke PR, Zhang C (2008). Spatial and temporal coordination of mitosis by Ran GTPase. Nat Rev Mol Cell Biol 9, 464–477.

Conti E, Muller CW, Stewart M (2006). Karyopherin flexibility in nucleocytoplasmic transport. Curr Opin Struct Biol 16, 237–244.

Conti E, Uy M, Leighton L, Blobel G, Kuriyan J (1998). Crystallographic analysis of the recognition of a nuclear localization signal by the nuclear import factor karyopherin alpha. Cell 94, 193–204.

Cronshaw JM, Krutchinsky AN, Zhang W, Chait BT, Matunis MJ (2002). Proteomic analysis of the mammalian nuclear pore complex. J Cell Biol 158, 915–927.

Cross M, Powers M (2008). In vitro nuclear assembly using fractionated *Xenopus* egg extracts. J Vis Exp 18, 908.

Cross MK, Powers MA (2009). Learning about cancer from frogs: analysis of mitotic spindles in *Xenopus* egg extracts. Dis Model Mech 2, 541–547.

Cross MK, Powers MA (2011). Nup98 regulates bipolar spindle assembly through association with microtubules and opposition of MCAK. Mol Biol Cell 22, 661–672.

Dasso M (2001). Running on Ran: nuclear transport and the mitotic spindle. Cell 104, 321–324.

Delmar VA, Chan RC, Forbes DJ (2008). *Xenopus* importin beta validates human importin beta as a cell cycle negative regulator. BMC Cell Biol 9, 14.

Di Fiore B, Ciciarello M, Lavia P (2004). Mitotic functions of the Ran GTPase network: the importance of being in the right place at the right time. Cell Cycle 3, 305–313.

Dormann D *et al.* (2012). ALS-associated fused in sarcoma (FUS) mutations disrupt transportin-mediated nuclear import. EMBO J 29, 2841–2857.

Ems-McClung SC, Zheng Y, Walczak CE (2004). Importin {alpha}/{beta} and Ran-GTP regulate XCTK2 microtubule binding through a bipartite nuclear localization signal. Mol Biol Cell 15, 46–57.

Finlay DR, Forbes DJ (1990). Reconstitution of biochemically altered nuclear pores: transport can be eliminated and restored. Cell 60, 17–29.

Forbes DJ, Kirschner MW, Newport JW (1983). Spontaneous formation of nucleus-like structures around bacteriophage DNA microinjected into *Xenopus* eggs. Cell 34, 13–23.

Fornerod M, Ohno M, Yoshida M, Mattaj IW (1997). CRM1 is an export receptor for leucine-rich nuclear export signals. Cell 90, 1051–1060.

Franz C, Walczak R, Yavuz S, Santarella R, Gentzel M, Askjaer P, Galy V, Hetzer M, Mattaj IW, Antonin W (2007). MEL-28/ELYS is required for the recruitment of nucleoporins to chromatin and postmitotic nuclear pore complex assembly. EMBO Rep 8, 165–172.

Frey S, Richter RP, Gorlich D (2006). FG-rich repeats of nuclear pore proteins form a three-dimensional meshwork with hydrogel-like properties. Science 314, 815–817.

Fried H, Kutay U (2003). Nucleocytoplasmic transport: taking an inventory. Cell Mol Life Sci 60, 1659–1688.

Galy V, Askjaer P, Franz C, Lopez-Iglesias C, Mattaj IW (2006). MEL-28, a novel nuclear-envelope and kinetochore protein essential for zygotic nuclear-envelope assembly in *C. elegans*. Curr Biol 16, 1748–1756.

Goldfarb DS, Corbett AH, Mason DA, Harreman MT, Adam SA (2004). Importin alpha: a multipurpose nuclear-transport receptor. Trends Cell Biol 14, 505–514.

Gorlich D, Kutay U (1999). Transport between the cell nucleus and the cytoplasm. Annu Rev Cell Dev Biol 15, 607–660.

Gorlich D, Pante N, Kutay U, Aebi U, Bischoff FR (1996). Identification of different roles for RanGDP and RanGTP in nuclear protein import. EMBO J 15, 5584–5594.

Gorlich D, Prehn S, Laskey RA, Hartmann E (1994). Isolation of a protein that is essential for the first step of nuclear protein import. Cell 79, 767–778.

Gorlich D, Rapoport TA (1993). Protein translocation into proteoliposomes reconstituted from purified components of the endoplasmic reticulum membrane. Cell 75, 615–630.

Gorlich D, Vogel F, Mills AD, Hartmann E, Laskey RA (1995). Distinct functions for the two importin subunits in nuclear protein import. Nature 377, 246–248.

Groves MR, Hanlon N, Turowski P, Hemmings BA, Barford D (1999). The structure of the protein phosphatase 2A PR65/A subunit reveals the conformation of its 15 tandemly repeated HEAT motifs. Cell 96, 99–110.

Gruss OJ, Carazo-Salas RE, Schatz CA, Guarguaglini G, Kast J, Wilm M, Le Bot N, Vernos I, Karsenti E, Mattaj IW (2001). Ran induces spindle assembly by reversing the inhibitory effect of importin alpha on TPX2 activity. Cell 104, 83–93.

Hachet V, Kocher T, Wilm M, Mattaj IW (2004). Importin alpha associates with membranes and participates in nuclear envelope assembly in vitro. EMBO J 23, 1526–1535.

Hahn S, Maurer P, Caesar S, Schlenstedt G (2008). Classical NLS proteins from *Saccharomyces cerevisiae*. J Mol Biol 379, 678–694.

Harel A, Chan RC, Lachish-Zalait A, Zimmerman E, Elbaum M, Forbes DJ (2003a). Importin beta negatively regulates nuclear membrane fusion and nuclear pore complex assembly. Mol Biol Cell 14, 4387–4396.

Harel A, Forbes DJ (2004). Importin beta: conducting a much larger cellular symphony. Mol Cell 16, 319–330.

Harel A, Orjalo AV, Vincent T, Lachish-Zalait A, Vasu S, Shah S, Zimmerman E, Elbaum M, Forbes DJ (2003b). Removal of a single pore subcomplex results in vertebrate nuclei devoid of nuclear pores. Mol Cell 11, 853–864.

Hetzer M, Gruss OJ, Mattaj IW (2002). The Ran GTPase as a marker of chromosome position in spindle formation and nuclear envelope assembly. Nat Cell Biol 4, E177–E184.

Hinshaw JE, Carragher BO, Milligan RA (1992). Architecture and design of the nuclear pore complex. Cell 69, 1133–1141.

Hintersteiner M *et al.* (2010). Identification of a small molecule inhibitor of importin beta mediated nuclear import by confocal on-bead screening of tagged one-bead one-compound libraries. ACS Chem Biol 5, 967–979.

Hua XH, Newport J (1998). Identification of a preinitiation step in DNA replication that is independent of origin recognition complex and cdc6, but dependent on cdk2. J Cell Biol 140, 271–281.

Hu C-K, Coughlin M, Mitchison TJ (2012). Midbody assembly and its regulation during cytokinesis. Mol Biol Cell 23, 1024–1034.

Iijima M, Suzuki M, Tanabe A, Nishimura A, Yamada M (2006). Two motifs essential for nuclear import of the hnRNP A1 nucleocytoplasmic shuttling sequence M9 core. FEBS Lett 580, 1365–1370.

Izaurralde E, Kutay U, von Kobbe C, Mattaj IW, Gorlich D (1997). The asymmetric distribution of the constituents of the Ran system is essential for transport into and out of the nucleus. EMBO J 16, 6535–6547.

Kalab P, Heald R (2008). The RanGTP gradient—a GPS for the mitotic spindle. J Cell Sci 121, 1577–1586.

Kalab P, Pralle A, Isacoff EY, Heald R, Weis K (2006). Analysis of a RanGTP-regulated gradient in mitotic somatic cells. Nature 440, 697–701.

Kalab P, Pu RT, Dasso M (1999). The Ran GTPase regulates mitotic spindle assembly. Curr Biol 9, 481–484.

Kalab P, Weis K, Heald R (2002). Visualization of a Ran-GTP gradient in interphase and mitotic *Xenopus* egg extracts. Science 295, 2452–2456.

Kehlenbach RH, Assheuer R, Kehlenbach A, Becker J, Gerace L (2001). Stimulation of nuclear export and inhibition of nuclear import by a Ran mutant deficient in binding to Ran-binding protein 1. J Biol Chem 276, 14524–14531.

Kehlenbach RH, Dickmanns A, Kehlenbach A, Guan T, Gerace L (1999). A role for RanBP1 in the release of CRM1 from the nuclear pore complex in a terminal step of nuclear export. J Cell Biol 145, 645–657.

Kimura M, Okumura N, Kose S, Takao T, Imamoto N (2013). Identification of cargo proteins specific for importin-β with importin-α applying a stable isotope labeling by amino acids in cell culture (SILAC)-based in vitro transport system. J Biol Chem 288, 24540–24549.

Kutay U, Hetzer MW (2008). Reorganization of the nuclear envelope during open mitosis. Curr Opin Cell Biol 20, 669–677.

Lachish-Zalait A, Lau CK, Fichtman B, Zimmerman E, Harel A, Gaylord MR, Forbes DJ, Elbaum M (2009). Transportin mediates nuclear entry of DNA in vertebrate systems. Traffic 10, 1414–1428.

Lau CK, Delmar VA, Chan RC, Phung Q, Bernis C, Fichtman B, Rasala BA, Forbes DJ (2009). Transportin regulates major mitotic assembly events: from spindle to nuclear pore assembly. Mol Biol Cell 20, 4043–4058.

Lee DC, Aitchison JD (1999). Kap104p-mediated nuclear import. Nuclear localization signals in mRNA-binding proteins and the role of Ran and Rna. J Biol Chem 274, 29031–29037.

Lee BJ, Cansizoglu AE, Suel KE, Louis TH, Zhang Z, Chook YM (2006). Rules for nuclear localization sequence recognition by karyopherin beta 2. Cell 126, 543–558.

Li HY, Wirtz D, Zheng Y (2003). A mechanism of coupling RCC1 mobility to RanGTP production on the chromatin in vivo. J Cell Biol 160, 635–644.

Lim RY, Ullman KS, Fahrenkrog B (2008). Biology and biophysics of the nuclear pore complex and its components. Int Rev Cell Mol Biol 267, 299–342.

Lohka MJ, Maller JL (1985). Induction of nuclear envelope breakdown, chromosome condensation, and spindle formation in cell-free extracts. J Cell Biol 101, 518–523.

Lohka MJ, Masui Y (1983). Formation in vitro of sperm pronuclei and mitotic chromosomes induced by amphibian ooplasmic components. Science 220, 719–721.

Loiodice I, Alves A, Rabut G, Van Overbeek M, Ellenberg J, Sibarita JB, Doye V (2004). The entire Nup107-160 complex, including three new members, is targeted as one entity to kinetochores in mitosis. Mol Biol Cell 15, 3333–3344.

Macaulay C, Forbes DJ (1996). Assembly of the nuclear pore: biochemically distinct steps revealed with NEM, GTP gamma S, and BAPTA. J Cell Biol 132, 5–20.

Mackay DR, Makise M, Ullman KS (2010). Defects in nuclear pore assembly lead to activation of an Aurora B-mediated abscission checkpoint. J Cell Biol 191, 923–931.

Mackay DR, Ullman KS (2011). Coordinating postmitotic nuclear pore complex assembly with abscission timing. Nucleus 2, 283–288.

Marelli M, Dilworth DJ, Wozniak RW, Aitchison JD (2001a). The dynamics of karyopherin-mediated nuclear transport. Biochem Cell Biol 79, 603–612.

Marelli M, Lusk CP, Chan H, Aitchison JD, Wozniak RW (2001b). A link between the synthesis of nucleoporins and the biogenesis of the nuclear envelope. J Cell Biol 153, 709–724.

Maresca TJ, Heald R (2006). Methods for studying spindle assembly and chromosome condensation in *Xenopus* egg extracts. Methods Mol Biol 322, 459–474.

Marshall IC, Wilson KL (1997). Nuclear envelope assembly after mitosis. Trends Cell Biol 7, 69–74.

Melchior F, Gerace L (1998). Two-way trafficking with Ran. Trends Cell Biol 8, 175–179.

Melchior F, Paschal B, Evans J, Gerace L (1993). Inhibition of nuclear protein import by nonhydrolyzable analogues of GTP and identification of the small GTPase Ran/TC4 as an essential transport factor. J Cell Biol 123, 1649–1659.

Mishra RK, Chakraborty P, Arnaoutov A, Fontoura BM, Dasso M (2010). The Nup107-160 complex and gamma-TuRC regulate microtubule polymerization at kinetochores. Nat Cell Biol 12, 164–169.

Moore W, Zhang C, Clarke PR (2002). Targeting of RCC1 to chromosomes is required for proper mitotic spindle assembly in human cells. Curr Biol 12, 1442–1447.

Mosammaparast N, Pemberton LF (2004). Karyopherins: from nuclear-transport mediators to nuclear-function regulators. Trends Cell Biol 14, 547–556.

Murray AW (1991). Cell cycle extracts. Methods Cell Biol 36, 581–605.

Nachury MV, Maresca TJ, Salmon WC, Waterman-Storer CM, Heald R, Weis K (2001). Importin beta is a mitotic target of the small GTPase Ran in spindle assembly. Cell 104, 95–106.

Nakielny S, Siomi MC, Siomi H, Michael WM, Pollard V, Dreyfuss G (1996). Transportin: nuclear transport receptor of a novel nuclear protein import pathway. Exp Cell Res 229, 261–266.

Nelson LM, Rose RC, Moroianu J (2002). Nuclear import strategies of high risk HPV16 L1 major capsid protein. J Biol Chem 277, 23958–23964.

Newmeyer DD, Wilson KL (1991). Egg extracts for nuclear import and nuclear assembly reactions. Methods Cell Biol 36, 607–634.

Newport J (1987). Nuclear reconstitution in vitro: stages of assembly around protein-free DNA. Cell 48, 205–217.

Newport J, Dunphy W (1992). Characterization of the membrane binding and fusion events during nuclear envelope assembly using purified components. J Cell Biol 116, 295–306.

Newport J, Spann T (1987). Disassembly of the nucleus in mitotic extracts: membrane vesicularization, lamin disassembly, and chromosome condensation are independent processes. Cell 48, 219–230.

Ohba T, Nakamura M, Nishitani H, Nishimoto T (1999). Self-organization of microtubule asters induced in *Xenopus* egg extracts by GTP-bound Ran. Science 284, 1356–1358.

Ohtsubo M, Okazaki H, Nishimoto T (1989). The RCC1 protein, a regulator for the onset of chromosome condensation locates in the nucleus and binds to DNA. J Cell Biol 109, 1389–1397.

Orjalo AV, Arnaoutov A, Shen Z, Boyarchuk Y, Zeitlin SG, Fontoura B, Briggs S, Dasso M, Forbes DJ (2006). The Nup107-160 nucleoporin complex is required for correct bipolar spindle assembly. Mol Biol Cell 17, 3806–3818.

Pfaller R, Smythe C, Newport JW (1991). Assembly/disassembly of the nuclear envelope membrane: cell cycle-dependent binding of nuclear membrane vesicles to chromatin in vitro. Cell 65, 209–217.

Pollard VW, Michael WM, Nakielny S, Siomi MC, Wang F, Dreyfuss G (1996). A novel receptor-mediated nuclear protein import pathway. Cell 86, 985–994.

Powers MA, Forbes DJ, Dahlberg JE, Lund E (1997). The vertebrate GLFG nucleoporin, Nup98, is an essential component of multiple RNA export pathways. J Cell Biol 136, 241–250.

Prunuske AJ, Ullman KS (2006). The nuclear envelope: form and reformation. Curr Opin Cell Biol 18, 108–116.

Quimby BB, Dasso M (2003). The small GTPase Ran: interpreting the signs. Curr Opin Cell Biol 15, 338–344.

Rasala BA, Orjalo AV, Shen Z, Briggs S, Forbes DJ (2006). ELYS is a dual nucleoporin/kinetochore protein required for nuclear pore assembly and proper cell division. Proc Natl Acad Sci USA 103, 17801–17806.

Rasala BA, Ramos C, Harel A, Forbes DJ (2008). Capture of AT-rich chromatin by ELYS recruits POM121 and NDC1 to initiate nuclear pore assembly. Mol Biol Cell 19, 3982–3996.

Rebane A, Aab A, Steitz JA (2004). Transportins 1 and 2 are redundant nuclear import factors for hnRNP A1 and HuR. RNA 10, 590–599.

Reichelt R, Holzenburg A, Buhle EL Jr, Jarnik M, Engel A, Aebi U (1990). Correlation between structure and mass distribution of the nuclear pore complex and of distinct pore complex components. J Cell Biol 110, 883–894.

Ren M, Drivas G, D'Eustachio P, Rush MG (1993). Ran/TC4: a small nuclear GTP-binding protein that regulates DNA synthesis. J Cell Biol 120, 313–323.

Ribbeck K et al. (2006). NuSAP, a mitotic RanGTP target that stabilizes and cross-links microtubules. Mol Biol Cell 17, 2646–2660.

Rotem A, Gruber R, Shorer H, Shaulov L, Klein E, Harel A (2009). Importin β regulates the seeding of chromatin with initiation sites for nuclear pore assembly. Mol Biol Cell 20, 4031–4042.

Rout MP, Aitchison JD, Suprapto A, Hjertaas K, Zhao Y, Chait BT (2000). The yeast nuclear pore complex: composition, architecture, and transport mechanism. J Cell Biol 148, 635–651.

Ryan KJ, McCaffery JM, Wente SR (2003). The Ran GTPase cycle is required for yeast nuclear pore complex assembly. J Cell Biol 160, 1041–1053.

Ryan KJ, Zhou Y, Wente SR (2007). The karyopherin Kap95 regulates nuclear pore complex assembly into intact nuclear envelopes in vivo. Mol Biol Cell 18, 886–898.

Sagata N, Watanabe N, Vande Woude GF, Ikawa Y (1989). The c-mos proto-oncogene product is a cytostatic factor responsible for meiotic arrest in vertebrate eggs. Nature 342, 512–518.

Sauer G, Körner R, Hanisch A, Ries A, Nigg EA, Silljé HHW (2005). Proteome analysis of the human mitotic spindle. Mol Cell Proteomics 4, 35–43.

Siomi H, Dreyfuss G (1995). A nuclear localization domain in the hnRNP A1 protein. J Cell Biol 129, 551–560.

Soderholm JF, Bird SL, Kalab P, Sampathkumar Y, Hasegawa K, Uehara-Bingen M, Weis K, Heald R (2011). Importazole, a small molecule inhibitor of the transport receptor importin-beta. ACS Chem Biol 6, 700–708.

Strawn LA, Shen T, Shulga N, Goldfarb DS, Wente SR (2004). Minimal nuclear pore complexes define FG repeat domains essential for transport. Nat Cell Biol 6, 197–206.

Suel KE, Gu H, Chook YM (2008). Modular organization and combinatorial energetics of proline-tyrosine nuclear localization signals. PLoS Biol 6, e137.

Tsai MY, Wang S, Heidinger JM, Shumaker DK, Adam SA, Goldman RD, Zheng Y (2006). A mitotic lamin B matrix induced by RanGTP required for spindle assembly. Science 311, 1887–1893.

Walde S, Kehlenbach RH (2010). The part and the whole: functions of nucleoporins in nucleocytoplasmic transport. Trends Cell Biol 20, 461–469.

Walther TC et al. (2003a). The conserved Nup107-160 complex is critical for nuclear pore complex assembly. Cell 113, 195–206.

Walther TC, Askjaer P, Gentzel M, Habermann A, Griffiths G, Wilm M, Mattaj IW, Hetzer M (2003b). RanGTP mediates nuclear pore complex assembly. Nature 424, 689–694.

Wandke C, Kutay U (2013). Enclosing chromatin: reassembly of the nucleus after open mitosis. Cell 152, 1222–1225.

Wente SR, Rout MP (2010). The nuclear pore complex and nuclear transport. Cold Spring Harb Perspect Biol 2, a000562.

Wiese C, Goldberg MW, Allen TD, Wilson KL (1997). Nuclear envelope assembly in *Xenopus* extracts visualized by scanning EM reveals a transport-dependent 'envelope smoothing' event. J Cell Sci 110, 1489–1502.

Wiese C, Wilde A, Moore MS, Adam SA, Merdes A, Zheng Y (2001). Role of importin-beta in coupling Ran to downstream targets in microtubule assembly. Science 291, 653–656.

Wilde A, Lizarraga SB, Zhang L, Wiese C, Gliksman NR, Walczak CE, Zheng Y (2001). Ran stimulates spindle assembly by altering microtubule dynamics and the balance of motor activities. Nat Cell Biol 3, 221–227.

Wilde A, Zheng Y (1999). Stimulation of microtubule aster formation and spindle assembly by the small GTPase Ran. Science 284, 1359–1362.

Wilson KL, Newport J (1988). A trypsin-sensitive receptor on membrane vesicles is required for nuclear envelope formation in vitro. J Cell Biol 107, 57–68.

Wood KW, Sakowicz R, Goldstein LS, Cleveland DW (1997). CENP-E is a plus end-directed kinetochore motor required for metaphase chromosome alignment. Cell 91, 357–366.

Xu D, Farmer A, Chook YM (2010). Recognition of nuclear targeting signals by karyopherin-beta proteins. Curr Opin Struct Biol 20, 782–790.

Yokoyama H, Gruss OJ, Rybina S, Caudron Mw, Schelder M, Wilm M, Mattaj IW, Karsenti E (2008). Cdk11 is a RanGTP-dependent microtubule stabilization factor that regulates spindle assembly rate. J Cell Biol 180, 867–875.

Zhang C, Goldberg MW, Moore WJ, Allen TD, Clarke PR (2002a). Concentration of Ran on chromatin induces decondensation, nuclear envelope formation and nuclear pore complex assembly. Eur J Cell Biol 81, 623–633.

Zhang C, Hughes M, Clarke PR (1999). Ran-GTP stabilises microtubule asters and inhibits nuclear assembly in *Xenopus* egg extracts. J Cell Sci 112, 2453–2461.

Zhang C, Hutchins JR, Muhlhausser P, Kutay U, Clarke PR (2002b). Role of importin-beta in the control of nuclear envelope assembly by Ran. Curr Biol 12, 498–502.

Zhang ZC, Chook YM (2012). Structural and energetic basis of ALS-causing mutations in the atypical proline-tyrosine nuclear localization signal of the fused in sarcoma protein (FUS). Proc Natl Acad Sci USA 109, 12017–12021.

Zuccolo M et al. (2007). The human Nup107-160 nuclear pore subcomplex contributes to proper kinetochore functions. EMBO J 26, 1853–1864.